Research Square

Preprints are preliminary reports that have not undergone peer review.
They should not be considered conclusive, used to inform clinical practice,
or referenced by the media as validated information.

In silico evaluation of broccoli and kale leaf extracts as xanthine oxidase inhibitors for gout therapy

Daniel Boison
University of Cape Coast
Josephine Anoa Barnor
University of Cape Coast
Stephen Asare Asamoah
University of Cape Coast
Ekow Sekyi Etwire
University of Cape Coast
Robertson Akrofi
University of Cape Coast
Meshack Antwi-Adjei
University of Cape Coast
Francis Ackah Armah
University of Cape Coast
Samuel Kojo Kwofie
University of Ghana
Michael Buenor Adinortey
University of Cape Coast
Patrick Opare Sakyi
patrick.sakyi@uenr.edu.gh

University of Energy and Natural Resources

Research Article

Keywords:

Posted Date: April 30th, 2026

DOI: https://doi.org/10.21203/rs.3.rs-9271389/v1

License: This work is licensed under a Creative Commons Attribution 4.0 International License. Read Full License

Additional Declarations: No competing interests reported.

Abstract

Background:

Xanthine oxidase (XO), a key enzyme in purine metabolism, catalyzes the oxidation of hypoxanthine to xanthine and subsequently, xanthine to uric acid, the final product of purine catabolism in humans. XO enzyme plays a critical role in controlling uric acid levels thus, targeting it, is essential in managing conditions like gout.

Objectives: This study is aimed at exploring the bioactive compounds in *Brassica oleracea* var. italica (broccoli) and *Brassica oleracea* var. acephala (kale) for their potential anti-gout properties and ability to inhibit XO through an *in-silico* approach.

Methodology: Broccoli and kale leaves were subjected to solvent extraction. Phytochemicals from the extracts were identified using GC-MS analysis and subsequently docked against the XO receptor. ADMET and medicinal chemistry analyses were conducted on selected compounds to assess their pharmacological and safety profiles, and molecular interactions with XO were evaluated.

Results: Out of the 28 compounds docked, seven showed favorable binding affinities, with binding energies below –7.0 kcal/mol. Among these, butylated hydroxytoluene and benzyl benzoate emerged as lead compounds, exhibiting favorable pharmacodynamic properties and minimal predicted toxicity. They interacted hydrophobically with key residues of the target protein and-showed a markedly inhibitory potential against XO.

Conclusion: Butylated hydroxytoluene and benzyl benzoate emerged as lead compounds and exhibited inhibitory effects against XO, suggestive of a therapeutic source for gout therapy.

INTRODUCTION

Gout has emerged as a notable public health issue worldwide, with a marked increase in both its prevalence and incidence in recent decades [1, 2]. It is classified as an inflammatory arthritis condition linked to elevated uric acid levels in the blood, a state known as hyperuricemia. The hyperuricemic condition leads to the deposition of urate crystals in the joints of various body parts such as the wrist, fingers, ankle, toe, and knee [3, 4], resulting in symptoms such as redness, tenderness, warmth, and swelling during acute inflammatory episodes [5].

The synthesis of uric acid occurs through the oxidation of purine metabolites, specifically hypoxanthine and xanthine, facilitated by the enzyme xanthine oxidase (XO) [6]. This molybdenum-dependent enzyme plays a crucial role in the degradation of purine nucleotides, catalyzing two key rate-limiting steps in this metabolic pathway [7, 8]. The enzymatic process involves several intricate steps, including the activation of the hydroxyl group of the molybdenum cofactor, nucleophilic attack on xanthine, and the formation of uric acid, all while managing electron flow through associated cofactors.

The conversion of xanthine to uric acid involves a series of four reaction steps facilitated by specific cofactors and amino acids. Initially, the proton from the hydroxyl group of the molybdenum cofactor (Moco) is transferred to Glu1261, which activates the hydroxyl group for a nucleophilic attack on xanthine. In this step, Glu802 plays a crucial role in stabilizing the negative charge of the intermediate formed. The second step involves the transfer of a hydride ion from the tetrahedral intermediate to the sulfur atom of Moco, resulting in the reduction of molybdenum from Mo (VI) to Mo (IV). Subsequently, in the third step, uric acid is produced through protonation by Arg880, with the assistance of a water molecule. The final step involves the reduction of FAD to $FADH_2$, which re-oxidizes Mo (IV) back to its original oxidation state, Mo (VI).

This enzymatic process is supported by two [2Fe-2S] clusters that connect the Moco and FAD cofactors, facilitating electron transfer. After the reaction cycle, the enzyme is reset by the interaction of a water molecule with Moco [9, 10]. Notably, the enzyme exhibits a decreased affinity for NAD + at the FAD site while showing an increased affinity for oxygen. This change promotes the transfer of one or two electrons to O_2, resulting in the formation of superoxide (O_2^-) and hydrogen peroxide (H_2O_2) [11].

It is clear that XO's activity is characterized by a reduced affinity for NAD^+ at the FAD site and an increased affinity for oxygen, which leads to the production of reactive oxygen species such as superoxide and hydrogen peroxide. This complex biochemical process underscores the importance of XO in the pathophysiology of gout and highlights it as a potential therapeutic target for managing this condition. Several studies have identified XO as a potential therapeutic target for controlling uric acid accumulation. Inhibitors of XO could be utilized as drugs to prevent the excessive production of uric acid by hindering the enzyme's over activity [12]. Management options for gout include the use of analgesics, non-steroidal anti-inflammatory drugs (NSAIDs), and XO inhibitors like allopurinol and febuxostat [13] used to lower serum uric acid levels [14]. However, none of the existing management options is without adverse effects, as they may cause gastrointestinal side effects such as diarrhea, nausea, and vomiting, especially at high doses, and have been associated with renal, cardiovascular, and hypersensitivity reactions [15].

Given the challenges associated with conventional drug discovery approaches, which are often slow and costly, there is a pressing need for alternative sources with minimal or no adverse effects for inflammatory disorders like gout. *In silico* investigations present a viable alternative for identifying potential small molecules that may be more effective in managing gout. Additionally, exploring medicinal plants with ethnopharmacological relevance could enhance the likelihood of discovering potential drug candidates.

Cruciferous vegetables, including broccoli, cabbage, cauliflower, kale, and brussels sprouts, are highly nutritious and contain various bioactive compounds [16]. Their regular consumption is linked to a reduced risk of several chronic diseases, such as diabetes mellitus, asthma, and Alzheimer’s disease. The health benefits attributed to these vegetables primarily stem from their rich content of phytonutrients, which include glucosinolates, polyphenols, carotenoids, and terpenoids (17). Notably, broccoli and kale are both part of the Brassicaceae family, which is one of the most extensively cultivated plant families globally [18].

Broccoli, scientifically known as *Brassica oleracea var. italica*, is a globally consumed vegetable known for its nutritional richness, particularly in vitamins such as C, E, and K, as well as several B vitamins. It also provides essential minerals and bioactive compounds, including various glucosinolates [19, 20], which are linked to health benefits such as antibacterial, cardioprotective, antioxidant activities and antifungal properties, as well as potential cancer growth inhibition [19–22].

Kale, also called *Brassica oleracea var. acephala*, is another important member of the Brassica family, recognized for its resilience and low production costs [23]. It is valued for its nutritional profile, which includes calcium, vitamin C, and various phytochemicals that contribute to its antioxidant and anti-cancer properties. Kale is often referred to as a superfood due to its high antioxidant capacity and the extensive research supporting its health benefits. The leaves and stems are valued for their medicinal and nutritional qualities [24]. Kale is recognized for its numerous health advantages, including antioxidant, anticancer, and protective effects on the cardiovascular and gastrointestinal systems [23, 25]. Its nutritional profile is rich, containing essential nutrients such as calcium, vitamin C, folate, riboflavin, anthocyanins, phenolic acid, flavonoids, and vitamin A [23, 25, 26]. Additionally, kale is noted for its high levels of glucosinolates, carotenoids, and phenolic compounds, which contribute to its pharmacological effects and antioxidant properties [23]. Ethnopharmacologically, *Brassica oleracea var. acephala* DC has been widely utilized for the treatment of gastric ulcers [27], and its phytoconstituents have proven to impede the activity of the spike glycoprotein trimer associated with SARS-CoV-2, suggesting their possible role in antiviral strategies against this virus [28]. Furthermore, it has been reported that secondary metabolites present in *Brassica oleracea var. italica* reduce the risk of several serious health conditions, including diabetes, cancer, and neurological disorder [29].

In silico pharmacological screening of the isolated compounds from *Brassica oleracea var. italica* and *Brassica oleracea var. acephala* could contribute to identifying new XO inhibitors derived from natural sources [30]. Therefore, this study employed an *in silico* approach, including molecular docking, to screen the bioactive compounds in *Brassica oleracea var. italica* and *Brassica oleracea* var. *acephala* against the protein receptor XO, assessing their potential anti-gout properties and ability to inhibit XO.

MATERIALS AND METHODS

Preparation of Plant Material

Fresh kale leaves and broccoli were purchased from the Abura market in Cape Coast, Ghana, on February 29, 2024. Both samples were washed under running tap water, air-dried at 50°C for fourteen (14) days, and pulverized using an electric blender. Each powdered sample was macerated with acetonitrile and diethyl ether in a 1:10 w/v ratio for seven (7) days. The macerate was filtered and concentrated using a rotary evaporator at 65°C for acetonitrile and 35°C for diethyl ether. The extraction of kale yielded 0.131g (0.873%) of extract and 0.466g (3.107%) of diethyl ether extract. In contrast, the extraction of broccoli resulted in 0.499g (3.327%) of acetonitrile extract and 0.854g (5.693%) of diethyl ether extract.

GC-MS identification of phytochemicals in Extracts

The bioactive compounds present in *Brassica oleracea* extracts were assessed using gas chromatography-mass spectrometry (GC-MS). The GC-MS analysis was conducted using a 7000C GC-MS triple quadrupole system equipped with a PAL autosampler for precise sample injection. An aliquot of 1.5 µL from each extract was dissolved in acetonitrile and diethyl ether before being injected into the GC-MS/MS system (Agilent Technologies, CA, USA). The GC oven temperature program began at 60°C, where it was held for 2 minutes. It then ramped up to 180°C at a rate of 20°C/min, with a 1-minute hold, before increasing further to 280°C at 5°C/min, eventually reaching a peak temperature of 325°C. The system utilized a splitless front inlet with helium as the carrier gas at a pressure of 17.729 psi and a total flow rate of 35 mL/min. An Agilent CP8944 VF-5ms column (30 m x 250 µm x 0.25 µm) was employed, starting with an initial flow rate of 2 mL/min, which decreased to 1.5 mL/min after the run. The mass spectrometer operated in electron ionization mode at 230°C, scanning from m/z 60 to 700, while the collision cell pressure was set to 3 psi, reducing to zero post-analysis. Helium and nitrogen were used as quench and collision gases, respectively, with flow rates of 2.25 mL/min and 1.5 mL/min. The bioactive compounds were identified by comparing their retention times and mass fragmentation patterns with those of known standards and a mass spectral library (MassHunter software). Quantification of the compounds was performed by measuring the peak areas.

In silico analysis

Retrieval and Preparation of the 3D Structure of Protein Receptor

The 3D crystal structure of XO, with a resolution of 2.5 Å, was obtained from the Protein Data Bank (www.rcsb.org, PDB ID: 1FIQ) in pdb format. The water molecules, heteroatoms, and co-crystallized ligands attached to the XO structure were removed using BIOVIA Discovery Studio 2024. Subsequently, polar hydrogen atoms were incorporated into the PDB file using the same software [31]. The missing residues were replaced on the protein structure, which was then subjected to energy minimization using SwissPDB viewer 4.1.0 (http://spdbv.unil.ch) [32].

Retrieval of Identified Ligands

The 2D conformer of the identified compounds in the extracts from the GC-MS/MS, as well as the reference drug allopurinol (PubChem ID 135401907), was downloaded from the PubChem Database (http://pubchem.ncbi.nlm.nih.gov) in the SDF (Structured Data Files) format [30].

Molecular Docking

PyRx 0.8.0.0 (https://pyrx.sourceforge.io), which integrates various open-source software tools like AutoDock, AutoDock Vina, and Open Babel, was utilized for the docking process. Prior to their conversion into AutoDock-compatible pdbqt format, the ligands were subjected to energy minimization using the universal force field through Open Babel [33]. The docking procedure was conducted with AutoDock Vina [31] to assess the binding affinity between XO and the compounds identified in Brassica oleracea extracts, utilizing the XYZ coordinates of the grid box that corresponds to the active site of the target protein,

centered at X: 21.1884 Å, Y: 16.3671 Å, and Z: 103.7037 Å, and with dimensions of 29.8485 × 24.8610 × 30.8403 Å [32]. The ligands were then ranked based on their binding affinity relative to the reference drugs.

Characterization of Binding Mechanism

Ligplot+ version 2.2.9 (www.ebi.ac.uk) was used to analyze the binding mechanisms between the target protein structure and the selected compounds. This program generates 2D schematic representations of protein-ligand complexes using structural data from the Protein Data Bank. It offers a clear and informative depiction of intermolecular interactions, including hydrogen bonds, hydrophobic interactions, and atom accessibility, along with an indication of interaction strength [34].

Validation of Docking Protocol

Validation of Docking Protocol
Validating the docking protocol is essential to ensure the accuracy and reliability of the docking results [35]. DockRMSD was utilized for this purpose (DockRMSD: Docking Pose Distance Calculation [zhanggroup.org]). The co-crystallized ligand was extracted from the protein receptor and re-docked into the energy-minimized protein. Both the co-crystallized and re-docked ligands were then converted to MOL2 file formats and input into DockRMSD to calculate the root mean square deviation (RMSD) between the two poses [36]. Using Ligplot+ version 2.2.9 (www.ebi.ac.uk), the co-crystallized and re-docked ligands were superimposed to identify the shared residues involved in ligand interactions [33].

Prediction of ADMET properties

The ADMET properties of the compounds with the top scores from the molecular docking studies were evaluated using SwissADME (www.swissadme.ch) and ADMETlab 3.0 (http://admetlab3.scbdd.com). Both SwissADME and ADMETlab 3.0 are valuable tools for drug discovery, providing comprehensive ADMET predictions and supporting the evaluation of potential drug candidates [37, 38]. They enable the computation of physicochemical properties and the prediction of pharmacokinetics, drug-likeness, and other therapeutic attributes [28]. The compounds were filtered using parameters such as Lipinski's rule of 5, bioavailability score, human intestinal absorption, nephrotoxicity, blood-brain barrier (BBB), drug-induced liver toxicity, Caco-2 permeability, pan-assay interference compounds (PAINS), half-life, and plasma clearance.

Biological Activity Prediction

PASS Online predicts over 3500 types of biological activities, such as pharmacological effects, toxic effects, interactions with enzymes, and changes in gene expression (https://www.way2drug.com/passonline/info.php#). It was employed to predict the biological activity of the selected compounds using the SMILES of the compounds as input. The software assesses compound activity by generating two probability values: probable activity (Pa) and probable inactivity (Pi). These values help predict the compound's activity profile, showing its potential to be either active or inactive [39].

Molecular Dynamic Simulations and MM-PBSA Calculations of the Protein-ligand complexes

Two of the hit compounds with the least binding energies with PubChem IDs, 31404 and 2345, as well as the known drug, allopurinol (PubChem ID: 135401907), serving as the control, were subjected to 100ns molecular dynamic simulations using GROMACS 2018 [40, 41]. The OPLS/All Atom force field [42] was first used to generate the topology and position restraint files for the target protein. Similarly, the topology and position restraint files of the three ligands were obtained using LigParGen [43]. To ensure that the surface atoms are not affected, which is normally caused by random particle movements, the protein-ligand complexes were restricted within a cubic simulation box, allowing a 1 nm gap from the edges. A single point charge was used to solvate the system, after which Na^+ or Cl^- ions were added for neutralization. Employing the steepest descent method with 50,000 steps, each system was energy minimized, followed by a 100ps equilibration. Ensembles of the number

of substances, volume, and temperature, as well as the number of substances, pressure, and temperature, were applied to ensure a well-equilibrated system was reached at 300 K and 1 bar of pressure. The output files obtained after the simulation, including root mean square deviation (RMSD), root mean square fluctuation (RMSF), and radius of gyration (Rg) trajectories, were plotted using Qtgrace [44]. MM-PBSA computations of the free binding energy and the per-residue energy contribution were calculated using MM/PBSA [45].

RESULTS

GC-MS Profiling of Phytochemicals in Brassica Extracts

A total of 16 compounds were detected in the acetonitrile and diethyl ether extracts of broccoli, while 12 compounds were identified in both extracts of kale. The analysis revealed 9 compounds in the diethyl ether extract (Table 1) and 7 compounds in the acetonitrile extract (Table 2) of broccoli, whereas 6 compounds were identified in each extract of kale (Tables 3 and 4). Arachidonic acid was present in both the acetonitrile and diethyl ether extracts of broccoli, while 1,4-benzenedicarboxylic acid, bis(2-ethylhexyl) ester, rhodopin, butylated hydroxytoluene, and fumaric acid, 1-cyclopentylethyl nonyl ester, were detected in both broccoli and kale extracts.

Table 1
Bioactive compounds identified in diethyl ether extract of broccoli.

Compound	RT (minutes)	Compound name	Area %	Molecular formula	Molecular weight(g/mol)
1	8.43	Butylated Hydroxytoluene	2.51	$C_{15}H_{24}O$	220.35
2	10.813	Benzyl Benzoate	0.91	$C_{14}H_{12}O_2$	212.24
3	15.806	Arachidonic acid	3.04	$C_{20}H_{32}O_2$	304.5
4	20.132	Hexadecamethyl-heptasiloxane,	0.74	$C_{16}H_{48}O_6Si_7$	533.1
5	22.267	Tetracosamethyl-cyclododecasiloxane	0.85	$C_{24}H_{72}O_{12}Si_{12}$	889.8
6	24.877	1,4- Benzenedicarboxylic acid, bis(2-ethylhexyl) ester	100	$C_{24}H_{38}O_4$	390.6
7	26.8	Pentyl octadecyl ether	6.93	$C_{23}H_{48}O$	340.6
8	29.157	Fumaric acid, 1- cyclopentylethyl nonyl ester	3.37	$C_{20}H_{34}O_4$	338.5
9	29.772	Eicosamethyl-cyclodecasiloxane,	1.15	$C_{20}H_{60}O_{10}Si_{10}$	741.5

Retention times (RT), peak areas, molecular formulas, and molecular weights are included.

Table 2
Bioactive compounds identified in acetonitrile extract of broccoli.

Compound	RT (minutes)	Compound name	Area %	Molecular formula	Molecular weight(g/mol)
1	4.181	Hematoporphyrin	36.09	$C_{34}H_{38}N_4O_6$	598.7
2	12.818	Lycoxanthin	18.6	$C_{40}H_{56}O$	552.9
3	13.118	Rhodopin	52.49	$C_{40}H_{58}O$	554.9
4	15.749	Arachidonic acid	100	$C_{20}H_{32}O_2$	304.5
5	16.049	4-Androsten-9.alpha.- fluoro-17.alpha.-methyl-3.alpha.,6.beta.,11.beta.,17.b eta.-tetra-ol, tetra-trimethylsily	18.5	$C_{32}H_{63}FO_4Si_4$	643.2
6	24.681	1,4- Benzenedicarboxylic acid, bis(2-ethylhexyl) ester	94.13	$C_{24}H_{38}O_4$	390.6
7	29.792	Vitamin E	31.24	$C_{29}H_{50}O_2$	430.7

Retention times (RT), peak areas, molecular formulas, and molecular weights are included.

Table 3
Bioactive compounds identified in diethyl ether extract of kale leaves.

Compound	RT (minutes)	Compound name	Area %	Molecular formula	Molecular weight(g/mol)
1	8.43	Butylated Hydroxytoluene	6.23	$C_{15}H_{24}O$	220.35
2	24.815	1,4-Benzenedicarboxylic acid, bis(2-ethylhexyl) ester	100	$C_{24}H_{38}O_4$	390.6
3	26.805	1-Decanol, 2-hexyl-	19	$C_{16}H_{34}O$	242.44
4	29.162	Fumaric acid, 1-cyclopentylethyl nonyl ester	10.39	$C_{20}H_{34}O_4$	338.5
5	29.42	Dasycarpidan-1-methanol, acetate (ester)	4.38	$C_{20}H_{26}N_2O_2$	326.4
6	15.739	Rhodopin	2.67	$C_{40}H_{58}O$	554.9

Retention times (RT), peak areas, molecular formulas, and molecular weights are included.

Table 4
Bioactive compounds identified in acetonitrile extract of kale leaves.

Compound	RT (minutes)	Compound name	Area %	Molecular formula	Molecular weight(g/mol)
1	5.194	Malic Acid	100	$C_4H_6O_5$	134.09
2	5.272	Butanoic acid, 2,3-dihydroxy propyl ester	13.78	$C_7H_{14}O_4$	162.18
3	11.304	Paraquat dichloride	8.83	$C_{12}H_{14}C_{l2}N_2$	257.16
4	13.154	Palmitic anhydride	12.03	$C_{32}H_{62}O_3$	494.8
5	15.837	Gorlic acid	16.12	$C_{18}H_{30}O_2$	278.4
6	24.706	1,4-Benzenedicarboxylic acid, bis(2-ethylhexyl) ester	32.32	$C_{24}H_{38}O_4$	390.6

Retention times (RT), peak areas, molecular formulas, and molecular weights are included.

Molecular Docking Analysis

To identify potential candidates for gout management, molecular docking studies were performed on 28 phytochemicals isolated from two *Brassica* species, with XO (PDB ID: 1FIQ) as the target. These compounds, along with the reference XO inhibitor allopurinol, were docked against the enzyme. Based on a binding energy threshold of − 7.0 kcal/mol [32, 46], seven (7) compounds demonstrated favorable binding affinities and were selected for further analysis. The binding energies of these ligands, in comparison with the reference drug, are summarized in Table 5. These top-performing compounds were subsequently subjected to downstream evaluations.

Table 5
Molecular docking results of the 28 phytochemicals

Broccoli			**Kale**		
Compound name	PubChem ID	Binding Energy(kcal/mol)	Compound name	PubChem ID	Binding Energy(kcal/mol)
Hematoporphyrin	11103	-9.7	Butylated Hydroxytoluene	31404	-10.4
Butylated Hydroxytoluene	31404	-10.4	1,4-Benzenedicarboxylic acid, bis(2-ethylhexyl) ester	22932	-7.9
Benzyl Benzoate	2345	-7.7	1-Decanol, 2-hexyl-	95337	-5.9
Arachidonic acid	444899	-6.6	Fumaric acid, 1-cyclopentylethyl nonyl ester	91736023	-6.9
Hexadecamethyl-heptasiloxane	10912	***	Dasycarpidan-1-methanol, acetate (ester)	550072	-7.9
Tetracosamethyl-cyclododecasiloxane	167767	***	Rhodopin	5365880	-6.0
1,4- Benzenedicarboxylic acid, bis(2-ethylhexyl) ester	22932	-7.9	Malic Acid	525	-5.2
Pentyl octadecyl ether	87077485	-6.3	Butanoic acid, 2,3-dihydroxy propyl ester	11188	-5.6
Fumaric acid, 1-cyclopentylethyl nonyl ester	91736023	-6.9	Paraquat dichloride	15938	-7.2
Eicosamethyl cyclodecasiloxane	519601	***	Palmitic anhydride	69339	-5.1
Lycoxanthin	5281245	-5.7	Gorlic acid	5282855	-5.7
Rhodopin	5365880	-6.0			
4-Androsten-9.alpha.- fluoro-17.alpha.-methyl-3.alpha.,6.beta.,11.beta.,17.beta.-tetra-ol, tetra-trimethylsily	91696616	***			
Vitamin E	2116	-10			
Reference drug					
Allopurinol	135401907	-6.4			

*Reference drug (used as a control), along with their binding energies. *** represents the silicon- containing phytochemicals.*

Validation of Docking Protocol

The structures of the re-docked and co-crystallized ligands were superimposed, and a root mean square deviation (RMSD) of 2.085 Å was computed. Docking poses with RMSD values ranging from 2.0 to 3.0 Å exhibit positional deviations from the reference structure; however, they retain the correct binding orientation [47]. This shows the accuracy and reliability of the docking results. When the co-crystallized and re-docked ligands were superimposed in Ligplot+, the 2D interaction analysis

revealed that 7 residues were common to both complexes. There was an overlap of two hydrogen bonds (with Phe798 and Met1038) and five hydrophobic interactions (with Arg912, Ser1080, Gln1040, Gly1039, and Gly1260). The observed overlaps demonstrate AutoDock Vina's effectiveness in reproducing the experimental binding conformation [33].

Drug Likeness.

Lipinski's rule assesses whether a biologically active compound possesses suitable chemical and physical properties for oral bioavailability [33]. The criteria include molecular weight ≤ 500 Da, LogP ≤ 5, hydrogen bond donors ≤ 5, hydrogen bond acceptors ≤ 10, and 40 ≤ molar refractivity ≤ 140 [32]. Among the seven compounds exhibiting high binding affinity, six (PubChem IDs: 2116, 2345, 22932, 550072, 31404, 15938) satisfied Lipinski's rule (Table 6). All six compounds demonstrated a bioavailability score of 0.55, further confirming their compliance with the rule. Additionally, none of the compounds triggered alerts for Pan-Assay Interference Compounds (PAINS), indicating the absence of substructures known to cause false-positive results in biological assays [48]. These six compounds were subsequently selected for downstream ADMET analyses. The reference drug also satisfied Lipinski's rule and showed no PAINS alerts.

Table 6
Medicinal chemistry properties of the 7 selected compounds in Brassica oleracea extracts and reference drug using Lipinski rule, bioavailability score and PAINS.

PubChem ID	Lipinski rule (Number of violations)	Bioavailability score	PAINS
2116	1	0.55	0 alerts
2345	0	0.55	0 alerts
22932	1	0.55	0 alerts
550072	0	0.55	0 alerts
31404	1	0.55	0 alerts
15938	0	0.55	0 alerts
11103	2	0.11	0 alerts
135401907	0	0.55	0 alerts

ADMET profiling

The ADMET evaluation of the investigated compounds provides valuable insights into their pharmacokinetic characteristics and safety profiles. The predicted ADMET parameters for the selected compounds are summarized in Table 7. Among the compounds assessed, Caco-2 permeability values indicated excellent absorption for PubChem IDs 2116, 2345, 22932, 550072, and 31404, with values of − 5.011, − 4.670, − 4.916, − 5.053, and − 4.987, respectively. PubChem ID 15938 exhibited poor Caco-2 permeability and was therefore excluded from further analysis. The reference drug also showed excellent permeability. Assessment of human intestinal absorption (HIA) corroborated these findings, with PubChem IDs 2116, 2345, 22932, 550072, and the reference drug all displaying excellent absorption profiles, while PubChem IDs 15938 and 31404 showed intermediate absorption levels. Evaluation of blood-brain barrier (BBB) permeability showed that PubChem IDs 22932, 2116, and 550072 were BBB-permeant, whereas PubChem IDs 31404, 2345, and the reference drug were BBB-impermeant. Due to the significance of BBB selectivity in drug design [49], the BBB-permeant compounds were excluded from further development. Pharmacokinetic profiling indicated moderate plasma clearance for PubChem IDs 31404, 2345, and the reference drug, with a medium half-life for PubChem IDs 31404 and 2345, and a poor half-life for the reference drug. For the toxicity parameters, which included nephrotoxicity and drug-induced liver injury (DILI), both PubChem ID 31404 and 2345 were non-nephrotoxic and exhibited no signs of hepatotoxicity. In contrast, the reference drug demonstrated a poor safety profile in

both toxicity parameters. Following completion of the ADMET evaluation, PubChem IDs 31404 and 2345 emerged as the most promising lead candidates, demonstrating favorable pharmacokinetic and toxicity profiles.

Table 7
ADMET Prediction of selected compounds and the reference drug.

ADMET properties	PubChem ID 2116	PubChem ID 2345	PubChem ID 22932	PubChem ID 550072	PubChem ID 31404	PubChem ID 15938	PubChem ID 135401907
Caco-2 permeability	Excellent	Excellent	Excellent	Excellent	Excellent	Poor	Excellent
Human Intestinal Absorption	High	High	High	High	Moderate	Moderate	High
BBB	Poor	Medium	Poor	poor	Excellent	Excellent	Excellent
Plasma clearance	Moderate	Moderate	Moderate	Moderate	Moderate	Moderate	Moderate
Half-life	Excellent	Medium	Medium	Poor	Medium	Poor	Poor
Nephrotoxicity	Excellent	Excellent	Excellent	Excellent	Excellent	Poor	Poor
Drug induced liver toxicity	Excellent	Excellent	Excellent	Excellent	Excellent	Poor	Poor

Molecular Interaction of Selected Ligand

The protein, together with the selected ligands, formed a complex and was run in Ligplot+ version 2.2.8 to assess the molecular interaction. The binding interactions between the ligands and protein were studied to determine the significant intermolecular bonds within the complexes. PubChem ID 31404 exhibited hydrophobic interactions with Lys1045, Ser1082, Thr1083, Gln1040, Gln767, Thr1077, Met1038, Arg912, Phe798, Gln1261, Gly1260, and Ser1080. It also formed a hydrogen bond with Gln1194 (2.85 Å) PubChem ID 2345 also displayed hydrophobic interactions with Glu802, Phe798, Gly799, Glu1261, Arg912, Gly1260, Gln1040, Gly1039, Ala1079, Ser1080, Gln1194, and Met1038. The reference drug formed two hydrogen bonds with Gln767 (bond length: 2.90 Å and 3.00 Å), one hydrogen bond with Glu802 (2.94 Å), and one with Thr1077 (3.06 Å). Additionally, it engaged in hydrophobic interactions with Phe914, Glu1261, Gly1260, Phe798, Gly799, Ser1080, Ala1078, and Met1038. These interactions collectively suggest a stable and favorable binding conformation within the protein's active site. A comparison of the molecular interactions revealed that the residues Phe798, Met1038, Gly1260, Ser1080, and Glu1261 were commonly involved in the binding of both lead compounds and the reference drug. These shared amino acids suggest conserved interaction sites within the protein's active pocket.

XO Inhibitory and Anti-Gout Predictions Using PASS

Using PASS (Prediction of Activity Spectra for Substances), the potential biological activities of the compounds were assessed, along with their respective probabilities of activity (Pa) and inactivity (Pi). For PubChem ID 31404, notable predicted activities included oxidoreductase inhibition, antioxidant effects, anti-inflammatory properties, kidney function stimulation, oxidizing action, anti-uremic activity, free radical scavenging, antiarthritic potential, xanthine dehydrogenase inhibition, gout treatment, uric acid excretion stimulation, and non-steroidal anti-inflammatory effects, with Pa scores spanning 0.118 to 0.806. Similarly, PubChem ID 2345 was associated with oxidoreductase inhibition, antioxidant behavior, anti-inflammatory action, kidney function stimulation, oxidizing effects, anti-uremic properties, free radical scavenging, antiarthritic activity, xanthine dehydrogenase inhibition, gout treatment, non-steroidal anti-inflammatory action, hypoxanthine phosphoribosyl transferase inhibition, renal failure treatment, and xanthine oxidase inhibition, displaying Pa values from 0.15 to 0.655.

Table 8
PASS-predicted biological activities of lead compounds, with probable activity (Pa) and inactivity (Pi) scores.

Compound	Biological activity	Probable activity (Pa)	Probable inactivity (Pi)
Butylated Hydroxytoluene	Anti-Inflammatory	0.806	0.006
	Kidney Function Stimulant	0.727	0.006
	Oxygen Scavenger	0.669	0.01
	Antioxidant	0.58	0.005
	Oxidoreductase Inhibitor	0.576	0.046
	Anti-uremic	0.502	0.005
	Free Radical Scavenger	0.484	0.011
	Non-Steroidal Anti-inflammatory Agent	0.444	0.017
	Oxidizing Agent	0.363	0.028
	Antiarthritic	0.324	0.118
	Uric Acid Excretion Stimulant	0.224	0.053
	Gout Treatment	0.195	0.062
	Xanthine Dehydrogenase Inhibitor	0.118	0.038
Benzyl Benzoate	Kidney Function Stimulant	0.655	0.020
	Oxidoreductase Inhibitor	0.618	0.031
	Oxygen Scavenger	0.548	0.036
	Oxidizing Agent	0.49	0.009
	Anti-uremic	0.457	0.008
	Anti-Inflammatory	0.459	0.07
	Non-Steroidal Anti-inflammatory Agent	0.311	0.04
	Hypoxanthine Phosphoribosyl transferase Inhibitor	0.215	0.018
	Xanthine Oxidase Inhibitor	0.217	0.023
	Free Radical Scavenger	0.224	0.059
	Antioxidant	0.175	0.074
	Renal Failure Treatment	0.135	0.043
	Xanthine Dehydrogenase Inhibitor	0.174	0.014
	Gout Treatment	0.15	0.11

MD Simulations

Molecular docking studies have mostly allowed high ligand flexibility, while the protein is maintained with limited or no flexibility to amino acids within the active site or residues close to the binding site pockets [50]. In addition, cryptic pockets of target proteins which can only be revealed by conformational changes, are difficult to explore during molecular docking [51].

Molecular dynamic (MD) simulations are therefore employed to complement results from molecular docking studies by mitigating these challenges. MD simulations provide, at the atomic level, the dynamic interactions of proteins in a complex with ligands, offering insights into binding energy, stability, and conformational changes [52]. Integration of this concept has become critical, as understanding of how proteins interact with drugs offers an opportunity in designing new and effective therapeutic agents. Based on the aforementioned, a 100ns MD simulation was executed, and the outcomes, the RMSD, RMSF, Rg, and hydrogen bond graphs, were plotted.

The RMSD, which measures the deviations of the protein backbone from the initial pose over time, was computed to examine the stability of the various complexes [53]. Complexes with RMSD lower than 3 Å are said to be stable [54], while those greater with high fluctuations are said to be unstable. The ligands, 31404, 2345, and the reference drug, 135401907, recorded an initial surge in RMSD (to a maximum of 0.24 Å) in the first 40s (Fig. 10a) before levelling off. A careful look at the RMSD graph shows that both 2345 and 135401907 showed an average RMSD of 0.2 Å, while 31404 had the highest 0.21 Å (Fig. 10a). Overall, all the selected hit compounds and the reference drug recorded an average RMSD lower than the threshold and therefore suggested that the hit compounds possess the potential of forming stable complexes with the target protein.

Rg was computed to evaluate the compactness of the protein-ligand complexes [55]. Notably, a high Rg connotes a decrease in compactness upon ligand binding, possibly resulting in protein unfolding, while a low Rg is an indication of an increased folding of the target protein [54, 55]. Both identified hit compounds, 31404 and 2345, recorded an average Rg of 2.8 nm, comparable to the reference, 315401907 [0.2785 nm] (Fig. 10b), suggesting the potential of the ligands enhancing protein folding upon binding. RMSF, a metric used to quantify the flexibility of amino acids within a protein, was computed to identify which residues are critical for ligand binding [55]. Amino acid residues within the binding pockets of the target protein are mostly flexible, which, upon interacting with ligands, show minimum fluctuations, recording low RMSF (54). From the RMSF graph, residues within the ranges 610–990, 1100–1200, and 1150–1220 (Fig. 10c) recorded low RMSF, indicating their involvement in ligand binding and hence suggested to contribute to complex stability. The number of hydrogen bonding interactions formed during the entire simulation period shows the reference compound, 315401907, formed four hydrogen bonds with the target protein, while 31404 formed one hydrogen bond with 2345, not recording any hydrogen bond formation (Fig. 10d). Overall, results from the RMSD, RMSF, Rg, and number of hydrogen bond formations suggest the selected hit compounds and reference drug formed stable complexes with the target protein.

Molecular Mechanics Poisson-Boltzmann Surface Area Computations of Free Binding Energy

MM-PBSA has become essential in computational drug development for predicting and ranking hit compounds, as it computes an accurate free binding energy (ΔG_{bind}) using *van der Waals* interactions energy (ΔG_{vdW}), electrostatic energy (ΔG_{ele}), polar solvation energy ($\Delta G_{pol,\ sol}$), and non-polar solvation energy (ΔG_{SASA}) [56]. Complementing molecular docking results with MM-PBSA calculations ensures that the identified hit compounds possess the potential of inhibiting the target protein in the absence of the experimental evaluation [57]. The hit compound, 31404, recorded the least ΔG_{bind} of − 12.183 kJ/mol (Table 9), lower than the reference compound, 135401907 (− 4.384 kJ/mol), suggesting that it forms a feasible and stable complex with the target protein. While $\Delta G_{pol,\ sol}$ is the worst contributor, the ΔG_{vdW}, ΔG_{ele}, and ΔG_{SASA} contributed favorable energies to the observed ΔG_{bind} values. Interestingly, the hit compound, 2345, recorded a ΔG_{bind} of + 3.323 kJ/mol (Table 9), suggesting it does not possess the potential of inhibiting XO. Results from the molecular docking and MM-PBSA computations suggest the potential of 135401907 for modulating XO worthy of further experimental evaluation.

Table 9
Computed free binding energies of the complexes of selected hit compounds and the reference drug

Complex	ΔG_{vdW} (kJ/mol)	ΔG_{ele} (kJ/mol)	$\Delta G_{pol,sol}$ (kJ/mol)	ΔG_{SASA} (kJ/mol)	ΔG_{bind} (kJ/mol)
31404	−21.240 ± 2.631	−0.700 ± 1.001	13.407 ± 3.814	−3.650 ± 5.030	−12.183 ± 4.997
2345	−0.005 ± 0.014	−0.017 ± 0.332	3.242 ± 5.279	0.103 ± 2.894	+ 3.323 ± 5.312
135401907	−12.827 ± 4.923	−0.772 ± 2.013	9.490 ± 5.604	−0.275 ± 1.126	−4.384 ± 2.702

The energy contribution of each amino acid to the ΔG_{bind} was evaluated using per-residue decomposition analysis. The per-residue decomposition studies identify which amino acid is critical for ligand binding, as those involved contribute the most to the ΔG_{bind}. Amino acid residues that contribute energies greater than + 5 kJ/mol or lower than − 5 kJ/mol are considered necessary for complex stability [58]. Interestingly, while all the amino acids present in the target protein contributed useful energies (Fig. 11) to ΔG_{bind}, none was able to meet the threshold. This notwithstanding, exploring the residues in the binding pocket still provides a means of developing anti-gout chemotypes targeting XO.

DISCUSSION

The present study was conducted to screen for XO inhibitors from *Brassica oleracea* extracts for the possible treatment of gout. Plants generate diverse secondary metabolites as defense compounds, serving as a rich source of bioactive small molecules with potential therapeutic applications [59]. Among the members of the family Brassiceae, the genus *Brassica* stands out as the most important, comprising several globally significant crop species such as *Brassica oleracea* L., *Brassica napus* L., and *Brassica rapa* L. Notably, *B. oleracea* is the primary vegetable species and includes widely consumed vegetables like kale, broccoli, cauliflower, Brussels sprouts, and both red and white cabbage [60]. They are recognized for their wide-ranging health-promoting effects [61].

The *in silico* analysis performed in this study offers important insights into the potential inhibitory effects of bioactive compounds found in *Brassica oleracea* extracts on XO. Molecular docking is a widely used approach in drug discovery that facilitates the identification of optimal ligand orientations within a protein's binding site and enables the prediction of their binding affinities [59]. Seven (7) compounds, hematoporphyrin, butylated hydroxytoluene, 1,4-benzenedicarboxylic acid bis(2-ethylhexyl) ester, benzyl benzoate, dasycarpidan-1-methanol acetate (ester), paraquat dichloride, and vitamin E, exhibited binding affinities surpassing the − 7.0 kcal/mol threshold, indicating stronger molecular interactions with the target enzyme compared to the reference drug, allopurinol, which displayed a binding affinity of − 6.4 kcal/mol. In docking studies, if a compound exhibits lower binding energy compared to the standard, it indicates that the compound has the potential to exhibit greater activity [62]. A lower binding energy value suggests a more favorable and stable interaction between the ligand and the protein receptor. The inability of silicon-containing compounds to dock successfully in AutoDock Vina may stem from several factors inherent to the software's limitations in handling such molecules. Our docking experiments revealed an important limitation when working with silicon-containing compounds. This technical constraint reflects the underlying force field design of AutoDock Vina, which was specifically parameterized for common biological atoms, including carbon, nitrogen, oxygen, sulfur, and hydrogen [63, 64]. Since AutoDock's atom typing is also case-sensitive, the recognition of unsupported elements such as "Si" fails entirely. While this design choice enables efficient docking of typical drug-like molecules, it necessarily excludes certain organometallic and organosilicon compounds from analysis. Such limitations are not unique to AutoDock Vina, as many widely used docking tools exhibit similar constraints when confronted with non-standard atomic types [65].

Data on the physicochemical properties of the selected ligands were gathered through pharmacological analysis, along with safety profiling to assess their potential risks and benefits. Lipinski's rule determines and defines the drug-likeness and druggability of a compound. The Rule of 5 (Ro5) guidelines help predict whether a compound is likely to be effective as an oral drug [66]. Due to the widespread acceptance of these guidelines in drug development, there is a reduced pursuit of compounds that violate two or more of the Ro5 criteria [67]. Hematoporphyrin (PubChem ID: 11103) presents two violations

of Lipinski's Rule of Five: its molecular weight exceeds the 500 Da threshold, and it possesses more than five hydrogen bond donors (NH or OH); therefore, it was excluded from downstream analysis due to poor drug-likeness. With only one violation of Lipinski's Rule observed in 1,4-benzenedicarboxylic acid bis(2-ethylhexyl) ester (PubChem ID: 22932), vitamin E (PubChem ID: 2116), and butylated hydroxytoluene (PubChem ID: 31404), and full compliance seen in dasycarpidan-1-methanol acetate (PubChem ID: 550072), benzyl benzoate (PubChem ID: 2345), and paraquat dichloride (PubChem ID: 15938), these compounds demonstrated favorable drug-like properties and warrant further biological investigation.

The bioavailability score (ABS) is assessed based on a compound's compliance with or deviation from Lipinski's Rule of Five. At biological pH, a compound is expected to achieve more than 10% bioavailability (F) in rats if it adheres to Lipinski's criteria, resulting in an ABS of 0.55, meaning there's a 55% probability that F will exceed 10% in rats. On the other hand, if the compound does not meet these criteria, the ABS decreases to 0.17, indicating only a 17% chance of the compound having bioavailability greater than 10% in rats [68]. The selected compounds had an ABS of 0.55, making them effective via the oral route. PAINS are groups of chemical compounds with similar structural features, which increases the likelihood of these compounds exhibiting activity (or being identified as "hits") in various tests [69]. PAINS compounds can lead to misleading results in drug discovery assays due to their tendency to exhibit nonspecific interactions or cause other undesirable effects unrelated to the intended target [70]. This can lead to the inefficient use of time and resources by focusing on compounds that are unlikely to develop into viable drug candidates. Hence, compounds with 0 PAINS alerts are reliable for further development into therapeutic agents.

The properties of absorption, distribution, metabolism, excretion, and toxicity (ADMET) are crucial to pharmaceutical drug design. It is frequently reported that the inability of drug candidates to meet the necessary ADMET standards is a common reason for their high failure rates during the development process [71]. *In silico* ADMET studies are expected to reduce the risk of late-stage attrition of drug development and to optimize screening and testing by looking at only the promising compounds [72]. First, the Caco-2 (Colon Adenocarcinoma 2) monolayer cell culture model, which is regarded as the "gold standard" for evaluating drug permeability, is widely used in drug discovery to predict human intestinal absorption [73]. Five out of six selected compounds exhibited Caco-2 permeability values greater than − 5.15 log cm/s, suggesting favorable absorption profiles in the human body and eventually could possess better ADMET profiles.

The blood-brain barrier (BBB) is a highly selective semipermeable barrier that tightly regulates the movement of ions, molecules, and cells between the blood and the central nervous system (CNS). It protects the neural tissues from toxins and pathogens [74]. One of the key challenges in drug design is determining whether a compound can cross the BBB. Drugs that act on the nervous system must be able to pass through the BBB to work effectively. In contrast, medications aimed at other body parts should ideally not cross the BBB to avoid potential psychotropic side effects [49]. Butylated hydroxytoluene and benzyl benzoate were predicted to be impermeable to the BBB, indicating limited central nervous system penetration and a potentially favorable safety profile.

Clearance is a key pharmacokinetic (PK) parameter, as it influences both the half-life of a drug (in conjunction with the volume of distribution) and its bioavailability (alongside oral absorption). It therefore plays a critical role in determining the dosing regimen, both the frequency of administration and the appropriate dose required for effective treatment [75]. The reference drug, allopurinol (PubChem ID: 134018), exhibited lower plasma clearance compared to butylated hydroxytoluene and benzyl benzoate. Efficient plasma clearance is essential for drug elimination and helps prevent drug accumulation in the body. The half-life of a drug impacts its duration of effect, the time it takes to achieve stable concentrations, and the period necessary for the drug to be eliminated from the body [76]. In this regard, allopurinol also demonstrated a shorter and less favorable half-life compared to butylated hydroxytoluene and benzyl benzoate, potentially reducing its therapeutic efficacy.

Nephrotoxicity arises when the kidneys fail to perform their detoxification and excretion functions effectively, resulting from damage or impairment caused by external or internal toxic substances [77]. Drug-induced liver Injury (DILI) is a harmful liver response triggered by exposure to pharmaceutical agents or other xenobiotics. It may occur as a predictable reaction to high doses of toxic substances or as an unpredictable, idiosyncratic event even at therapeutic doses. DILI poses a significant challenge in drug development and clinical therapy, as genetic and environmental factors can alter drug metabolism and

excretion, leading to cellular stress, immune activation, and potentially severe liver damage. Its occurrence highlights the importance of evaluating liver toxicity during early stages of drug screening to ensure patient safety and regulatory compliance [78]. Butylated hydroxytoluene and benzyl benzoate were found to be neither hepatotoxic nor nephrotoxic, suggesting a favorable safety profile in contrast to the reference drug. Following ADMET profiling, butylated hydroxytoluene and benzyl benzoate emerged as promising lead candidates, underscoring their promise for further development, although experimental validation through *in vitro* and *in vivo* studies remains essential.

The biological activity spectrum was introduced to define the characteristics of substances that exhibit biological activity [79]. The predictive accuracy of the software, PASS, differs across various biological activities. Biological activities with Pa > Pi are considered worthy of pharmacological evaluation [32]. If the value of Pa exceeds 0.7, the substance is likely to demonstrate activity in experiments and has a high probability of being similar to an existing pharmaceutical agent. When Pa is between 0.5 and 0.7, the substance may still show activity, but with a lower likelihood, and it is less likely to resemble known pharmaceutical agents. If Pa falls below 0.5, the substance is unlikely to exhibit activity in experiments; however, if an activity is observed, it could indicate the discovery of a new chemical entity [79]. Butylated hydroxytoluene exhibited anti-inflammatory activity with a Pa value of 0.806, indicating its potential relevance for treating gout, an inflammatory form of arthritis [3]. Additionally, it showed kidney function stimulant activity with a Pa value of 0.727, suggesting a high likelihood of experimental validation, as values above 0.7 are generally considered predictive of true biological activity. A kidney function stimulant enhances the activity of the kidneys so it can effectively filter the blood and excrete waste substances like uric acid, which is primarily excreted through urine [80]. Benzyl benzoate exhibited oxidoreductase inhibitor activity with a Pa value of 0.618, suggesting a likelihood of inhibiting xanthine oxidoreductase in an experimental setting, though with a lower probability. Research has demonstrated a close association between the development of hyperuricemia or gouty arthritis and the production of reactive oxygen species (ROS) [81]. Antioxidants help reduce reactive oxygen species (ROS) levels and decrease oxidative stress [82]. Providing antioxidant support to patients with active gout may be a viable treatment strategy [83]. It is therefore not surprising that butylated hydroxytoluene and benzyl benzoate could prevent redox imbalance, suggesting potential antioxidant activity crucial for gout therapy.

Several activities, including XO inhibition, gout treatment, anti-uremic, antiarthritic, and others, showed Pa values below 0.5, suggesting a low probability of being confirmed in experimental settings. However, if these activities are validated in future studies, butylated hydroxytoluene and benzyl benzoate could represent novel therapeutic candidates. XO inhibitors are not solely restricted to the treatment of hyperuricemia and gout; evidence suggests that they can also be effective in addressing cardiovascular diseases [84].

The interaction between the protein and the lead compounds (i.e., butylated hydroxytoluene and benzyl benzoate) was predominantly governed by hydrophobic forces. Hydrophobic interactions are crucial contributors to the binding strength between drug candidates and their molecular targets. Studies indicate that prioritizing these interactions, even over traditional hydrogen bonding, can markedly influence the biological performance of lead compounds [85]. They are widely recognized as the principal thermodynamic driving force governing the association of small molecules with their protein receptors [86]. Moreover, increasing the number of hydrophobic atoms within the binding region of the drug-target complex has been associated with enhanced biological activity and therapeutic potential [85]. It was shown that butylated hydroxytoluene and benzyl benzoate portrayed higher hydrophobic interactions with their target molecules, indicating stronger biological activity with marked therapeutic effects.

Glu802 and Glu1261 are recognized as key catalytic residues within the active site of XO, playing central roles in substrate binding and the enzymatic conversion of xanthine to uric acid [9]. In this study, butylated hydroxytoluene and benzyl benzoate were found to interact with these critical residues, indicating their potential to modulate enzyme activity. Given the beneficial properties of butylated hydroxytoluene and benzyl benzoate, it is essential and worthwhile to explore their potential therapeutic effects, as they could be highly significant for the treatment of gout.

CONCLUSION

Overall, butylated hydroxytoluene and benzyl benzoate emerged as promising lead candidates to inhibit XO and serve as potential anti-gout agents. Following molecular docking, medicinal chemistry evaluation, and ADMET analyses, these compounds, identified as the most potent inhibitors from *Brassica oleracea var. italica* and *Brassica oleracea var. acephala*, demonstrated good binding affinities, high hydrophobic interactions, XO inhibitory activities, as well as a relative safety profile, and could possess a better ADMET profile. Inhibitors like butylated hydroxytoluene and benzyl benzoate present promising potential as alternatives or complementary agents to synthetic drugs such as allopurinol, offering the added benefit of potentially reduced side effects. These findings underscore the therapeutic potential of *Brassica oleracea* as a valuable source of natural xanthine oxidase inhibitors and highlight the need for further *in vitro* and *in vivo* studies to validate their clinical efficacy.

Abbreviations

ADMET	Absorption, Distribution, Metabolism, Excretion, and Toxicity
BBB	Blood-Brain Barrier
H-bond	Hydrogen bond
MD	Molecular Dynamics
PDB	Protein Data Bank
SDF	Structure Data File
SMILES	Simplified Molecular Input Line Entry System
MM-PBSA	Molecular Mechanics Poisson–Boltzmann Surface Area
XO	Xanthine oxidase
ABS	Bioavailability score
PASS	Prediction of Activity Spectra for Substances
GC-MS	Gas chromatography-mass spectrometry
PAINS	Pan-Assay Interference Compounds
RMSD	Root mean square deviation
RMSF	Root mean square fluctuation
CNS	Central Nervous System

Declarations

Ethics approval and consent to participate

Not Applicable.

Competing interests

The authors declare no conflicts of interest.

Data availability

Authors have provided all the data required in the manuscript. Any additional data are available upon request from the corresponding author.

Consent for publication

Not applicable.

Clinical Trial Number

Not applicable

Funding

This research received no external funding.

Acknowledgement

The West African Centre for Cell Biology of Infectious Pathogens, University of Ghana provided the high-performance computing platform (Zuputo) for running the molecular dynamic simulations and the MM-PBSA computations.

Authors' contributions

DB: conceptualization, supervision, methodology, data curation, validation, investigation, data analysis, Writing – original draft, review & editing, approved manuscript.

JAB: Data curation, investigation, methodology, data analysis, Writing - review & editing, approved manuscript.

SAA: Data analysis, investigation, Writing - review & editing, approved manuscript.

ESA: Data curation, investigation, data analysis, Writing - review & editing, approved manuscript.

RA: Data analysis, Writing - review & editing, approved manuscript.

MAA: methodology, investigation, validation, data analysis, Writing - original draft, review & editing, approved manuscript.

FAA: Data analysis, Writing - review & editing, approved manuscript.

SKK: Investigation, data analysis, Writing - review & editing, approved manuscript.

MBA: conceptualization, supervision, data analysis, methodology, investigation, Writing - original draft, review & editing, approved manuscript.

POS: conceptualization, supervision, methodology, investigation, validation, data analysis, Writing - original draft, review & editing, approved manuscript.

References

1. Han, T., Chen, W., Qiu, X., & Wang, W. (2024). Epidemiology of gout–Global burden of disease research from 1990 to 2019 and future trend predictions. *Therapeutic advances in endocrinology and metabolism*, 15, 20420188241227295. https://doi.org/10.1177/20420188241227295
2. Jin, Z., Wang, Z., Wang, R., Xiang, S., Zhang, W., Tang, Y. ... & Lv, S. (2024). Global burden and epidemic trends of gout attributable to high body mass index from 1990 to 2019. *Archives of Medical Science: AMS*, 20(1), 71. doi:10.5114/aoms/175469
3. Kuo, C. F., Grainge, M. J., Zhang, W., & Doherty, M. (2015). Global epidemiology of gout: prevalence, incidence and risk factors. *Nature reviews rheumatology*, 11(11), 649-662. doi:10.1038/nrrheum.2015.91
4. Yip, K., & Berman, J. (2021). What is gout?. *Jama,* 326(24), 2541-2541.doi:10.1001/jama.2021.19770
5. Jin, M., Yang, F., Yang, I., Yin, Y., Luo, J. J., Wang, H., & Yang, X. F. (2012). Uric acid, hyperuricemia and vascular diseases. *Frontiers in bioscience: a journal and virtual library*, 17, 656. doi: 10.2741/3950

6. Sekizuka, H. (2022). Uric acid, xanthine oxidase, and vascular damage: potential of xanthine oxidoreductase inhibitors to prevent cardiovascular diseases. *Hypertension Research*, 45(5), 772-774. doi:10.1038/s41440-022-00891-7
7. Furuhashi, M. (2020). New insights into purine metabolism in metabolic diseases: role of xanthine oxidoreductase activity. *American Journal of Physiology-Endocrinology and Metabolism*, 319(5), E827-E834. doi:10.1152/ajpendo.00378.2020
8. Harrison, R. (2002). Structure and function of xanthine oxidoreductase: where are we now?. *Free Radical Biology and Medicine*, 33(6), 774-797. doi:10.1016/S0891-5849(02)00956-5
9. Cao, H., Pauff, J. M., & Hille, R. (2010). Substrate orientation and catalytic specificity in the action of xanthine oxidase: the sequential hydroxylation of hypoxanthine to uric acid. *Journal of Biological Chemistry*, 285(36), 28044-28053. doi:10.1074/jbc.M110.128561
10. Ribeiro, P. M., Fernandes, H. S., Maia, L. B., Sousa, S. F., Moura, J. J., & Cerqueira, N. M. (2021). The complete catalytic mechanism of xanthine oxidase: a computational study. *Inorganic Chemistry Frontiers*, 8(2), 405-416. doi:10.1039/D0QI01029D
11. Cantu-Medellin, N., & Kelley, E. E. (2013). Xanthine oxidoreductase-catalyzed reactive species generation: a process in critical need of reevaluation. *Redox biology*, 1(1), 353-358. doi:10.1016/j.redox.2013.05.002
12. Nawaz, M. Z., Ain, Q. U., Zahid, S., Zulfiqar, T., Attique, S. A., Bilal, M. ... & Iqbal, H. M. (2020). Physicochemical features and structural analysis of xanthine oxidase as a potential therapeutic target to prevent gout. *Journal of Radiation Research and Applied Sciences*, 13(1), 616-628. doi:10.1080/16878507.2020.1812807
13. White, W. B. (2018). Gout, xanthine oxidase inhibition, and cardiovascular outcomes. *Circulation*, 138(11), 1127-1129. doi:10.1161/CIRCULATIONAHA.118.036148
14. Centers for Disease Control and Prevention. Gout [Internet]. 2023 [cited 2024 Mar 14]. Report No. Available from: https://www.cdc.gov/arthritis/gout/index.html
15. Suresh, E., & Das, P. (2012). Recent advances in management of gout. QJM: *An International Journal of Medicine*, 105(5), 407-417. doi:10.1093/qjmed/hcr242
16. Canbey, İ., Çınar, A. Y., Yıldız, E., & Gürbüz, O. (2022). Functional properties and health benefits of cruciferous vegetables. *Food Health and Technology Innovations*, 5(11), 452-462. https://izlik.org/JA49MH32KB
17. Ağagündüz, D., Şahin, T. Ö., Yılmaz, B., Ekenci, K. D., Duyar Özer, Ş., & Capasso, R. (2022). Cruciferous vegetables and their bioactive metabolites: from prevention to novel therapies of colorectal cancer. *Evidence-Based Complementary and Alternative Medicine*, 2022(1), 1534083. doi:10.1155/2022/1534083
18. Olsen, H., Grimmer, S., Aaby, K., Saha, S., & Borge, G. I. A. (2012). Antiproliferative effects of fresh and thermal processed green and red cultivars of curly kale (*Brassica oleracea L. convar. acephala var. sabellica*). *Journal of agricultural and food chemistry*, 60(30), 7375-7383. doi:10.1021/jf300875f
19. Nagraj, G. S., Chouksey, A., Jaiswal, S., & Jaiswal, A. K. (2020). Broccoli. In Nutritional composition and antioxidant properties of fruits and vegetables (pp. 5-17). Academic Press. doi:10.1016/B978-0-12-812780-3.00001-5
20. Vasanthi, H. R., Mukherjee, S., & Das, D. K. (2009). Potential health benefits of broccoli-a chemico-biological overview. *Mini reviews in medicinal chemistry*, 9(6), 749-759. doi:10.2174/138955709788452685
21. Latté, K. P., Appel, K. E., & Lampen, A. (2011). Health benefits and possible risks of broccoli–an overview. *Food and Chemical Toxicology*, 49(12), 3287-3309. doi:10.1016/j.fct.2011.08.019
22. Moreno, D. A., Carvajal, M., López-Berenguer, C., & García-Viguera, C. (2006). Chemical and biological characterization of nutraceutical compounds of broccoli. *Journal of pharmaceutical and biomedical analysis*, 41(5), 1508-1522. doi:10.1016/j.jpba.2006.04.003
23. Ortega-Hernández, E., Antunes-Ricardo, M., & Jacobo-Velázquez, D. A. (2021). Improving the health-benefits of kales (*Brassica oleracea L. var. acephala* DC) through the application of controlled abiotic stresses: *A review. Plants*, 10(12), 2629. doi:10.3390/plants10122629

24. Khalid, W., Iqra, Afzal, F., Rahim, M. A., Abdul Rehman, A., Faiz ul Rasul, H. ... & Refai, M. (2023). Industrial applications of kale (*Brassica oleracea var. sabellica*) as a functional ingredient: A review. *International Journal of Food Properties*, 26(1), 489-501. doi:10.1080/10942912.2023.2168011
25. Ayaz, F. A., Hayırlıoglu-Ayaz, S., Alpay-Karaoglu, S., Grúz, J., Valentová, K., Ulrichová, J., & Strnad, M. (2008). Phenolic acid contents of kale (*Brassica oleraceae L. var. acephala* DC.) extracts and their antioxidant and antibacterial activities. *Food Chemistry*, 107(1), 19-25. doi:10.1016/j.foodchem.2007.07.003
26. Šamec, D., Urlić, B., & Salopek-Sondi, B. (2019). Kale (*Brassica oleracea var. acephala*) as a superfood: Review of the scientific evidence behind the statement. *Critical reviews in food science and nutrition*, 59(15), 2411-2422. doi:10.1080/10408398.2018.1454400
27. Lemos, M., Santin, J. R., Júnior, L. C. K., Niero, R., & De Andrade, S. F. (2011). Gastroprotective activity of hydroalcoholic extract obtained from the leaves of *Brassica oleracea var. acephala* DC in different animal models. *Journal of ethnopharmacology*, 138(2), 503-507. doi:10.1016/j.jep.2011.09.046
28. Jose, S., Gupta, M., Sharma, U., Quintero-Saumeth, J., & Dwivedi, M. (2022). Potential of phytocompounds from *Brassica oleracea* targeting S2-domain of SARS-CoV-2 spike glycoproteins: Structural and molecular insights. *Journal of Molecular Structure*, 1254, 132369. doi:10.1016/j.molstruc.2022.132369
29. Kamboj, A., Sharma, S., Singh, V. P., Sinha, A., Yadav, K. S., Lal, B. ... & Devi, L. (2023). Phytochemical and therapeutic potential of broccoli (*Brassica oleracea*): A review. *Pharma Innov. J*, 12, 633-638.
30. Ghallab, D. S., Shawky, E., Metwally, A. M., Celik, I., Ibrahim, R. S., & Mohyeldin, M. M. (2022). Integrated in silico–in vitro strategy for the discovery of potential xanthine oxidase inhibitors from Egyptian propolis and their synergistic effect with allopurinol and febuxostat. *RSC advances*, 12(5), 2843-2872. doi:10.1039/D1RA08011C
31. Baskaran, K. P., Arumugam, A., Kandasamy, R., & Alagarsamy, S. (2020). *In silico* method for prediction of maximum binding affinity and ligand-protein interaction studies on Alzheimer's disease. *Int. J. Res. Granthaalayah*, 8(11), 362-370. doi:10.29121/granthaalayah.v8.i11.2020.2472
32. Kwofie, S. K., Annan, D. G., Adinortey, C. A., Boison, D., Kwarko, G. B., Abban, R. A., & Adinortey, M. B. (2022). Identification of novel potential inhibitors of varicella-zoster virus thymidine kinase from ethnopharmacologic relevant plants through an *in-silico* approach. *Journal of Biomolecular Structure and Dynamics*, 40(23), 12932-12947. doi:10.1080/07391102.2021.1977700
33. Adams, L., Afiadenyo, M., Kwofie, S. K., Wilson, M. D., Kusi, K. A., Obiri-Yeboah, D. ... & McKeon-Bennett, M. (2023). *In silico* screening of phytochemicals from *Dissotis rotundifolia* against Plasmodium falciparum Dihydrofolate Reductase. *Phytomedicine Plus*, 3(2), 100447. doi:10.1016/j.phyplu.2023.100447
34. Wallace, A. C., Laskowski, R. A., & Thornton, J. M. (1995). LIGPLOT: a program to generate schematic diagrams of protein-ligand interactions. *Protein engineering, design and selection*, 8(2), 127-134. doi:10.1093/protein/8.2.127
35. Umar, H. I., Josiah, S. S., Saliu, T. P., Jimoh, T. O., Ajayi, A., & Danjuma, J. B. (2021). *In-silico* analysis of the inhibition of the SARS-CoV-2 main protease by some active compounds from selected African plants. *Journal of Taibah University Medical Sciences*, 16(2), 162-176. doi:10.1016/j.jtumed.2020.12.005
36. Mateev, E., Valkova, I., Angelov, B., Georgieva, M., & Zlatkov, A. (2022). Validation through re-docking, cross-docking and ligand enrichment in various well-resoluted MAO-B receptors. *Int. J. Pharm. Sci. Res*, 13(3), 1000-1007. doi.org/10.13040/IJPSR.0975-8232
37. Daina, A., Michielin, O., & Zoete, V. (2017). SwissADME: a free web tool to evaluate pharmacokinetics, drug-likeness and medicinal chemistry friendliness of small molecules. *Scientific reports*, 7(1), 42717. doi:10.1038/srep42717
38. Fu, L., Shi, S., Yi, J., Wang, N., He, Y., Wu, Z. ... & Cao, D. (2024). ADMETlab 3.0: an updated comprehensive online ADMET prediction platform enhanced with broader coverage, improved performance, API functionality and decision support. *Nucleic acids research*, 52(W1), W422-W431. doi:10.1093/nar/gkae236
39. Chy, M. N. U., Chakrabarty, N., Roy, A., Paul, A., Emu, K. A., Dutta, T. ... & Tasnim, S. M. (2019). Antibacterial, anthelmintic, and analgesic activities of Piper sylvaticum (Roxb.) leaves and in silico molecular docking and PASS prediction studies of

its isolated compounds. *Journal of Complementary and Integrative Medicine*, 16(4), 20180176. doi:10.1515/jcim-2018-0176

40. Abraham, M. J., Murtola, T., Schulz, R., Páll, S., Smith, J. C., Hess, B., & Lindahl, E. (2015). GROMACS: High performance molecular simulations through multi-level parallelism from laptops to supercomputers. *SoftwareX*, 1, 19-25. doi:10.1016/J.SOFTX.2015.06.001
41. Van Der Spoel, D., Lindahl, E., Hess, B., Groenhof, G., Mark, A. E., & Berendsen, H. J. (2005). GROMACS: fast, flexible, and free. *Journal of computational chemistry*, 26(16), 1701-1718. doi:10.1002/JCC.20291
42. Siu, S. W., Pluhackova, K., & Böckmann, R. A. (2012). Optimization of the OPLS-AA force field for long hydrocarbons. *Journal of Chemical theory and Computation*, 8(4), 1459-1470. doi:10.1021/ct200908r
43. Jorgensen, W. L., & Tirado-Rives, J. (2005). Potential energy functions for atomic-level simulations of water and organic and biomolecular systems. *Proceedings of the National Academy of Sciences*, 102(19), 6665-6670. doi:10.1073/pnas.0408037102
44. Dahiya, R., Mohammad, T., Gupta, P., Haque, A., Alajmi, M. F., Hussain, A., & Hassan, M. I. (2019). Molecular interaction studies on ellagic acid for its anticancer potential targeting pyruvate dehydrogenase kinase 3. *RSC advances*, 9(40), 23302-23315. doi:10.1039/C9RA02864A
45. Kumari, R., Kumar, R., Open Source Drug Discovery Consortium, & Lynn, A. (2014). g_mmpbsa A GROMACS tool for high-throughput MM-PBSA calculations. J*ournal of chemical information and modeling*, 54(7), 1951-1962. doi:10.1021/ci500020m
46. Prasanth, D. S. N. B. K., Murahari, M., Chandramohan, V., Panda, S. P., Atmakuri, L. R., & Guntupalli, C. (2021). *In silico* identification of potential inhibitors from Cinnamon against main protease and spike glycoprotein of SARS CoV-2. *Journal of Biomolecular Structure and Dynamics*, 39(13), 4618-4632. doi:10.1080/07391102.2020.1779129
47. Ramírez, D., & Caballero, J. (2018). Is it reliable to take the molecular docking top scoring position as the best solution without considering available structural data?. *Molecules*, 23(5), 1038. doi:10.3390/molecules23051038
48. Xiong, G., Wu, Z., Yi, J., Fu, L., Yang, Z., Hsieh, C. ... & Cao, D. (2021). ADMETlab 2.0: an integrated online platform for accurate and comprehensive predictions of ADMET properties. *Nucleic acids research*, 49(W1), W5-W14. doi:10.1093/nar/gkab255
49. Carpenter, T. S., Kirshner, D. A., Lau, E. Y., Wong, S. E., Nilmeier, J. P., & Lightstone, F. C. (2014). A method to predict blood-brain barrier permeability of drug-like compounds using molecular dynamics simulations. *Biophysical journal*, 107(3), 630-641. doi:10.1016/j.bpj.2014.06.024
50. Guedes, I. A., de Magalhães, C. S., & Dardenne, L. E. (2014). Receptor–ligand molecular docking. *Biophysical reviews*, 6(1), 75-87. doi:10.1007/s12551-013-0130-2
51. Cimermancic, P., Weinkam, P., Rettenmaier, T. J., Bichmann, L., Keedy, D. A., Woldeyes, R. A. ... & Sali, A. (2016). CryptoSite: expanding the druggable proteome by characterization and prediction of cryptic binding sites. J*ournal of molecular biology*, 428(4), 709-719. doi:10.1016/J.JMB.2016.01.029
52. Sasidharan, S., Gosu, V., Tripathi, T., & Saudagar, P. (2023). Molecular dynamics simulation to study protein conformation and ligand interaction. In Protein folding dynamics and stability: experimental and computational methods (pp. 107-127). *Singapore: Springer Nature* Singapore. doi:10.1007/978-981-99-2079-2_6
53. Prabhakaran, P., Hebbani, A. V., Menon, S. V., Paital, B., Murmu, S., Kumar, S., ... & Desai, P. P. D. (2023). *In silico* generation of novel ligands for the inhibition of SARS-CoV-2 main protease (3CLpro) using deep learning. *Frontiers in microbiology*, 14, 1194794. doi:10.3389/fmicb.2023.1194794
54. Ashley, C. N., Broni, E., Pena-Martinez, M., Wood, C. M., Kwofie, S. K., & Miller III, W. A. (2025). Computer-Aided Discovery of Natural Compounds Targeting the ADAR2 dsRBD2-RNA Interface and Computational Modeling of Full-Length ADAR2 Protein Structure. *International Journal of Molecular Sciences*, 26(9), 4075. doi:10.3390/IJMS26094075/S1
55. Sakyi, P. O., Kwofie, S. K., Tuekpe, J. K., Gwira, T. M., Broni, E., Miller III, W. A., ... & Amewu, R. K. (2023). Inhibiting Leishmania donovani sterol methyltransferase to identify lead compounds using molecular modelling. *Pharmaceuticals*, 16(3), 330. doi:10.3390/ph16030330

56. Huang, K., Luo, S., Cong, Y., Zhong, S., Zhang, J. Z., & Duan, L. (2020). An accurate free energy estimator: based on MM/PBSA combined with interaction entropy for protein–ligand binding affinity. *Nanoscale*, 12(19), 10737-10750. doi:10.1039/C9NR10638C

57. Ganesan, A., Coote, M. L., & Barakat, K. (2017). Molecular dynamics-driven drug discovery: leaping forward with confidence. *Drug discovery today*, 22(2), 249-269. doi:10.1016/J.DRUDIS.2016.11.001

58. Kwofie, S. K., Dolling, N. N., Donkoh, E., Laryea, G. M., Mosi, L., Miller III, W. A. ... & Wilson, M. D. (2021). Pharmacophore-guided identification of natural products as potential inhibitors of *Mycobacterium ulcerans* cystathionine γ-synthase MetB. *Computation*, 9(3), 32. doi:10.3390/computation9030032

59. Adetutu, A., Olaniyi, T. D., & Owoade, O. A. (2021). GC-MS analysis and in silico assessment of constituents of Psidium guajava leaf extract against DNA gyrase of *Salmonella enterica* serovar Typhi. *Informatics in Medicine Unlocked*, 26, 100722. doi:10.1016/j.imu.2021.100722

60. Kapusta-Duch, J., Kopec, A., Piatkowska, E., Borczak, B., & Leszczynska, T. (2012). The beneficial effects of Brassica vegetables on human health. *Roczniki Państwowego Zakładu Higieny*, 63(4).

61. Shankar, S., Segaran, G., Sundar, R. D. V., Settu, S., & Sathiavelu, M. (2019). Brassicaceae-A classical review on its pharmacological activities. *Int. J. Pharm. Sci. Rev. Res*, 55(1), 107-113.

62. Madeswaran, A., Umamaheswari, M., Asokkumar, K., Sivashanmugam, T., Subhadradevi, V., & Jagannath, P. (2011). Docking studies: *In silico* lipoxygenase inhibitory activity of some commercially available flavonoids. *Bangladesh Journal of Pharmacology*, 6(2), 133-138. doi:10.3329/bjp.v6i2.9408

63. Huey, R., Morris, G. M., Olson, A. J., & Goodsell, D. S. (2007). A semiempirical free energy force field with charge-based desolvation. J*ournal of computational chemistry*, 28(6), 1145-1152. doi:10.1002/jcc.20634

64. Trott, O., & Olson, A. J. (2010). AutoDock Vina: improving the speed and accuracy of docking with a new scoring function, efficient optimization, and multithreading. *Journal of computational chemistry*, 31(2), 455-461. doi:10.1002/jcc.21334

65. Forli, S., Huey, R., Pique, M. E., Sanner, M. F., Goodsell, D. S., & Olson, A. J. (2016). Computational protein–ligand docking and virtual drug screening with the AutoDock suite. *Nature protocols*, 11(5), 905-919. doi:10.1038/nprot.2016.051

66. Morak-Młodawska, B., Jeleń, M., Martula, E., & Korlacki, R. (2023). Study of lipophilicity and ADME properties of 1, 9-diazaphenothiazines with anticancer action. *International journal of molecular sciences*, 24(8), 6970. doi:10.3390/ijms24086970

67. Benet, L. Z., Hosey, C. M., Ursu, O., & Oprea, T. I. (2016). BDDCS, the Rule of 5 and drugability. *Advanced drug delivery reviews*, 101, 89-98. doi:10.1016/j.addr.2016.05.007

68. Sharma, P., & Shanavas, A. (2021). Natural derivatives with dual binding potential against SARS-CoV-2 main protease and human ACE2 possess low oral bioavailability: a brief computational analysis. *Journal of Biomolecular Structure and Dynamics*, 39(15), 5819-5830. doi:10.1080/07391102.2020.1794970

69. Baell, J. B., & Nissink, J. W. M. (2018). Seven-Year Itch: Pan-Assay Interference Compounds (PAINS) in 2017- Utility and Limitations. *ACS chemical biology*, 13(1), 36-44. doi:10.1021/acschembio.7b00903

70. Sun, J., Zhong, H., Wang, K., Li, N., & Chen, L. (2021). Gains from no real PAINS: Where 'Fair Trial Strategy'stands in the development of multi-target ligands. *Acta Pharmaceutica Sinica B*, 11(11), 3417-3432. doi:10.1016/j.apsb.2021.02.023

71. Venkatraman, V. (2021). FP-ADMET: a compendium of fingerprint-based ADMET prediction models. *Journal of cheminformatics*, 13(1), 75. doi:10.1186/s13321-021-00557-5

72. Chakravarthi, P. V., Karthikeyan, M., Lakshmanan, L., Murugesan, S., Arivuchelvan, A., Sukumar, K. ... & Jagadeeswaran, A. (2023). Computational study of *Piper betle* L. phytocompounds by *in silico* and ADMET analysis for prediction of potential xanthine oxidase inhibitory activity. *BioRxiv*, 2023-01. doi:10.1101/2023.01.13.523909

73. Falcón-Cano, G., Molina, C., & Cabrera-Pérez, M. Á. (2022). Reliable prediction of Caco-2 permeability by supervised recursive machine learning approaches. *Pharmaceutics*, 14(10), 1998. doi:10.3390/pharmaceutics14101998

74. Daneman, R., & Prat, A. (2015). The blood–brain barrier. *Cold Spring Harbor perspectives in biology*, 7(1), a020412. doi:10.1101/cshperspect.a020412

75. Berellini, G., Waters, N. J., & Lombardo, F. (2012). *In silico* prediction of total human plasma clearance. *Journal of chemical information and modeling*, 52(8), 2069-2078. doi:10.1021/ci300155y
76. Andrade, C. (2022). The practical importance of half-life in psychopharmacology. *The Journal of Clinical Psychiatry*, 83(4), 22f14584-22f14584. doi:10.4088/JCP.22f14584
77. Kim, S. Y., & Moon, A. (2012). Drug-induced nephrotoxicity and its biomarkers. *Biomolecules & therapeutics*, 20(3), 268. doi:10.4062/biomolther.2012.20.3.268
78. Andrade, R. J., Chalasani, N., Björnsson, E. S., Suzuki, A., Kullak-Ublick, G. A., Watkins, P. B., ... & Aithal, G. P. (2019). Drug-induced liver injury. *Nature reviews Disease primers*, 5(1), 58. doi:10.1038/s41572-019-0105-0
79. Lagunin, A., Stepanchikova, A., Filimonov, D., & Poroikov, V. (2000). PASS: prediction of activity spectra for biologically active substances. *Bioinformatics*, 16(8), 747-748. doi:10.1093/bioinformatics/16.8.747
80. Bobulescu, I. A., & Moe, O. W. (2012). Renal transport of uric acid: evolving concepts and uncertainties. *Advances in chronic kidney disease*, 19(6), 358-371.doi:10.1053/j.ackd.2012.07.009
81. Zhang, S., Li, D., Fan, M., Yuan, J., Xie, C., Yuan, H. ... & Gao, H. (2024). Mechanism of reactive oxygen species-guided immune responses in gouty arthritis and potential therapeutic targets. *Biomolecules*, 14(8), 978. doi:10.3390/biom14080978
82. Kumar, S., Saxena, J., Srivastava, V. K., Kaushik, S., Singh, H., Abo-EL-Sooud, K. ... & Saluja, R. (2022). The interplay of oxidative stress and ROS scavenging: antioxidants as a therapeutic potential in sepsis. *Vaccines*, 10(10), 1575. doi:10.3390/vaccines10101575
83. Balik, A. R., Omma, A., & Sandikci, S. C. (2022). Evaluation of oxidative stress in gout disease; thiol-disulfide homeostasis and ischemia-modified albumin levels. *Int J Med Biochem*, 2022;5(2), 109-115 doi:10.14744/ijmb.2022.52714
84. Ali, H. I., Fujita, T., Akaho, E., & Nagamatsu, T. (2010). A comparative study of AutoDock and PMF scoring performances, and SAR of 2-substituted pyrazolotriazolopyrimidines and 4-substituted pyrazolopyrimidines as potent xanthine oxidase inhibitors. J*ournal of computer-aided molecular design*, 24(1), 57-75. doi:10.1007/s10822-009-9314-z
85. Patil, R., Das, S., Stanley, A., Yadav, L., Sudhakar, A., & Varma, A. K. (2010). Optimized hydrophobic interactions and hydrogen bonding at the target-ligand interface leads the pathways of drug designing. *PloS one*, 5(8), e12029. doi:10.1371/journal.pone.0012029
86. Young, T., Abel, R., Kim, B., Berne, B. J., & Friesner, R. A. (2007). Motifs for molecular recognition exploiting hydrophobic enclosure in protein–ligand binding. *Proceedings of the National Academy of Sciences*, 104(3), 808-813. https://doi.org/10.1073/pnas.0610202104

Figures

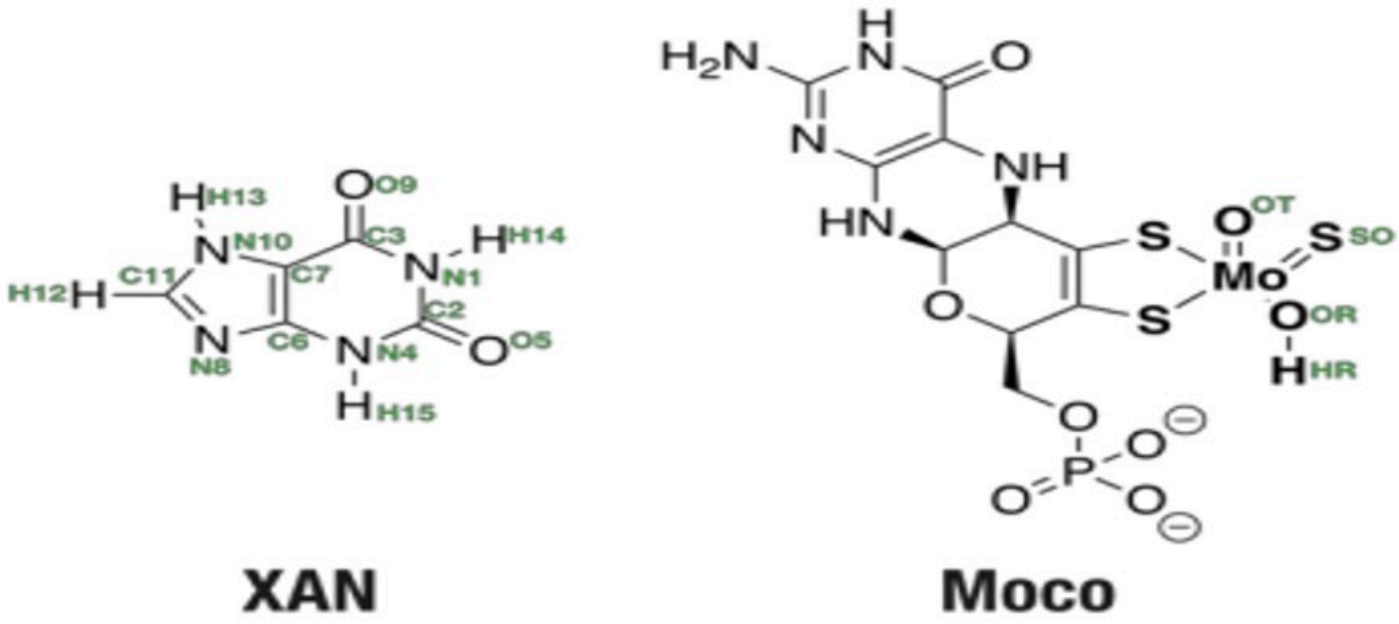


Figure 1

An illustration of the chemical structure of Moco and Xanthine molecules.

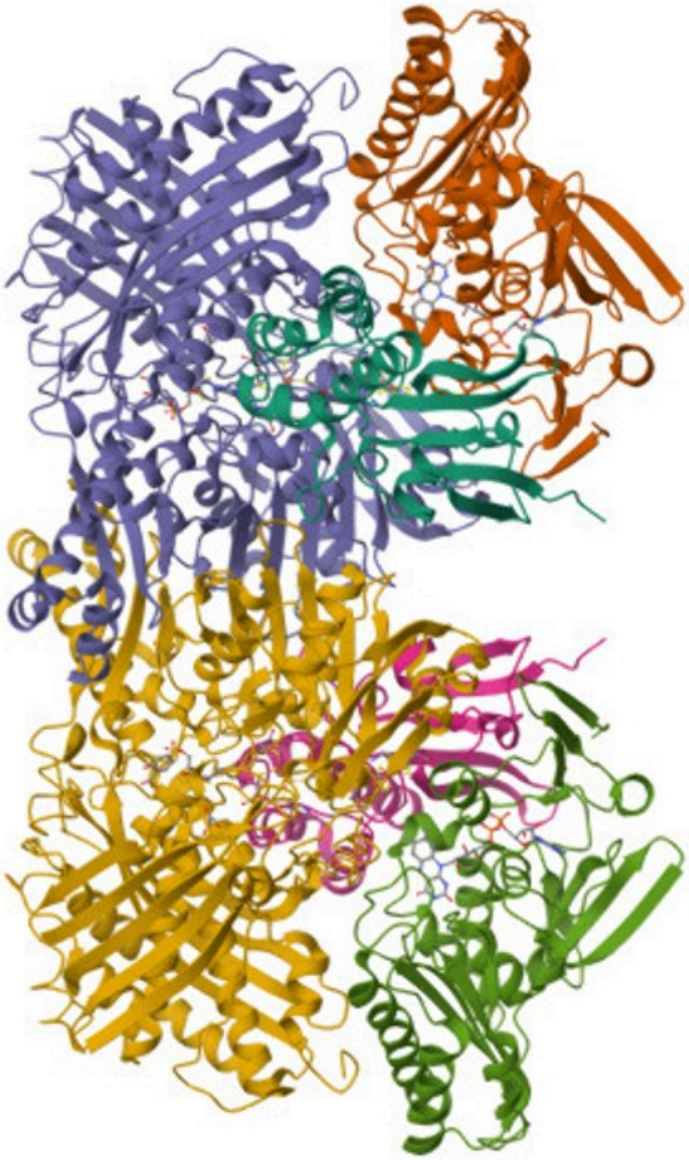


Figure 2

3D crystal structure of XO retrieved from Protein Data Bank https://cdn.rcsb.org/images/structures/1fiq_assembly-1.jpeg

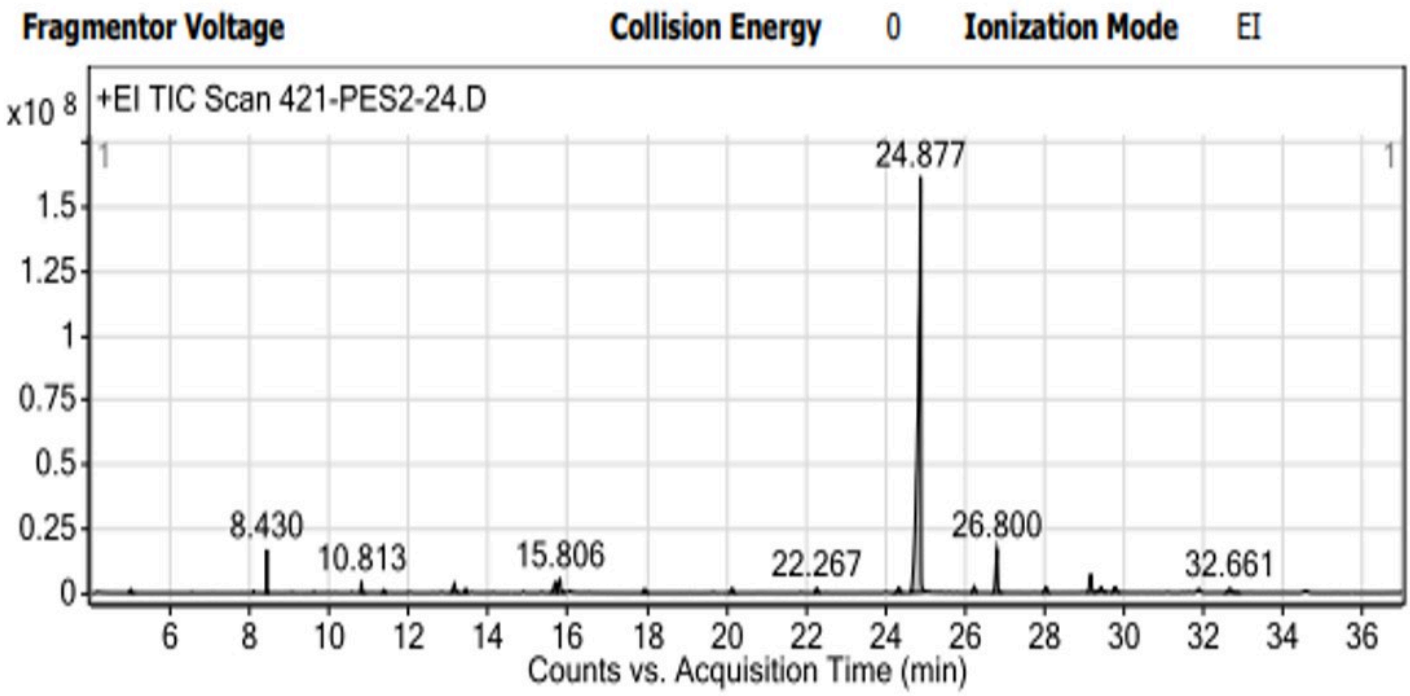


Figure 3

A chromatogram of the retention times of the compounds present in the diethyl ether extract of broccoli.

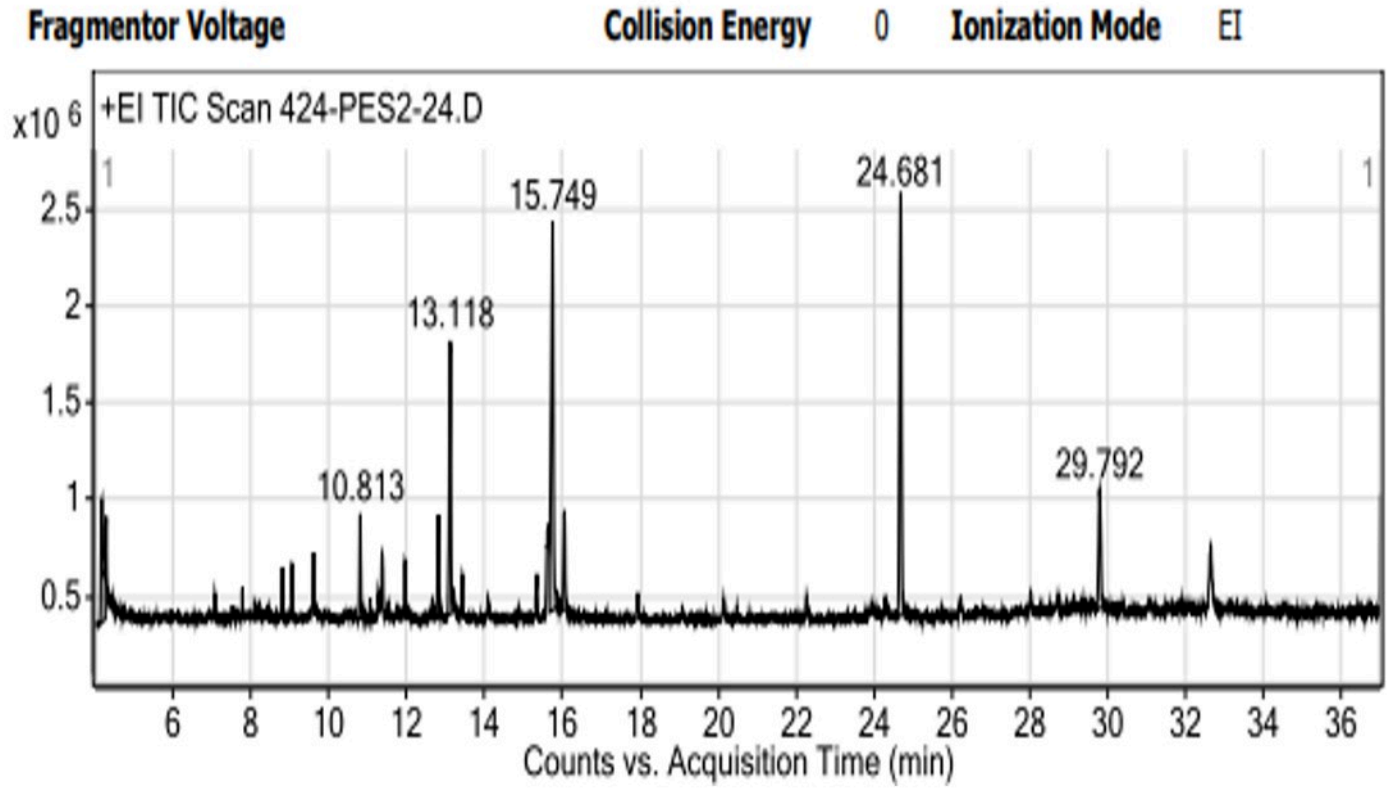


Figure 4

A chromatogram of the retention times of the compounds present in the acetonitrile extract of broccoli.

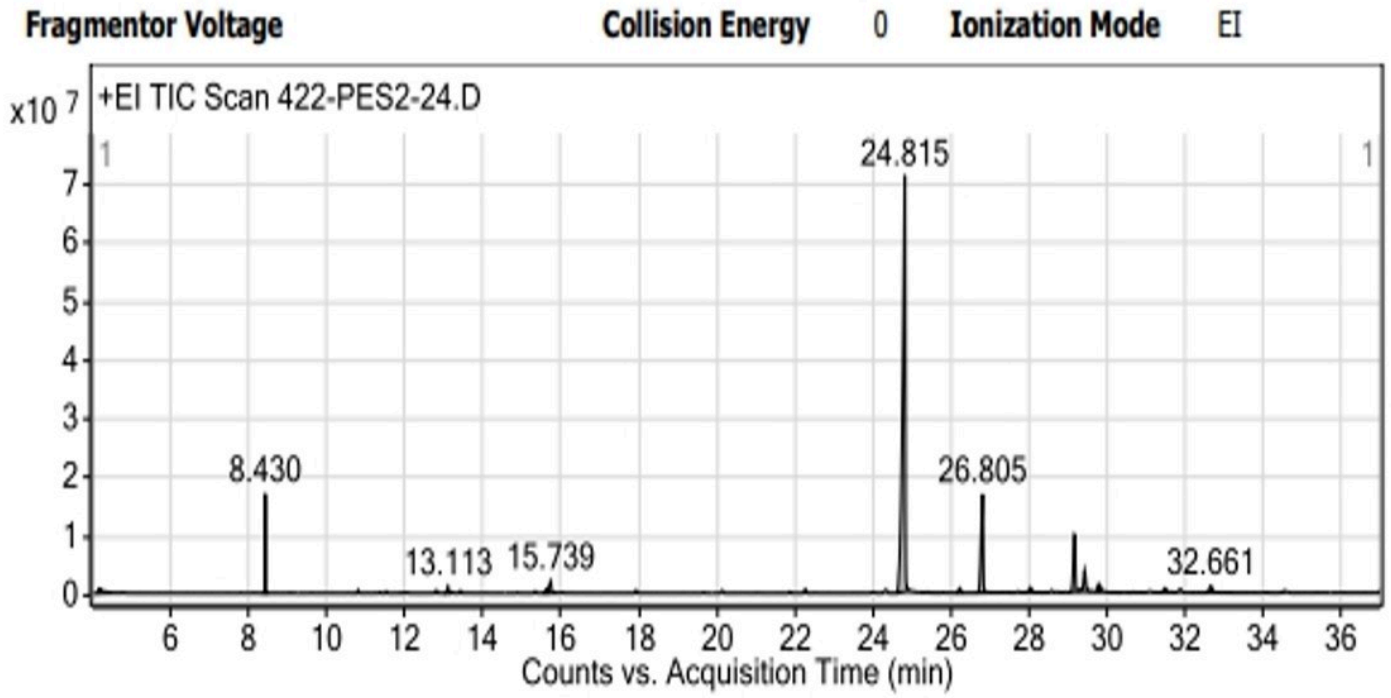


Figure 5

A chromatogram of the retention times of the compounds present in the diethyl ether extract of kale.

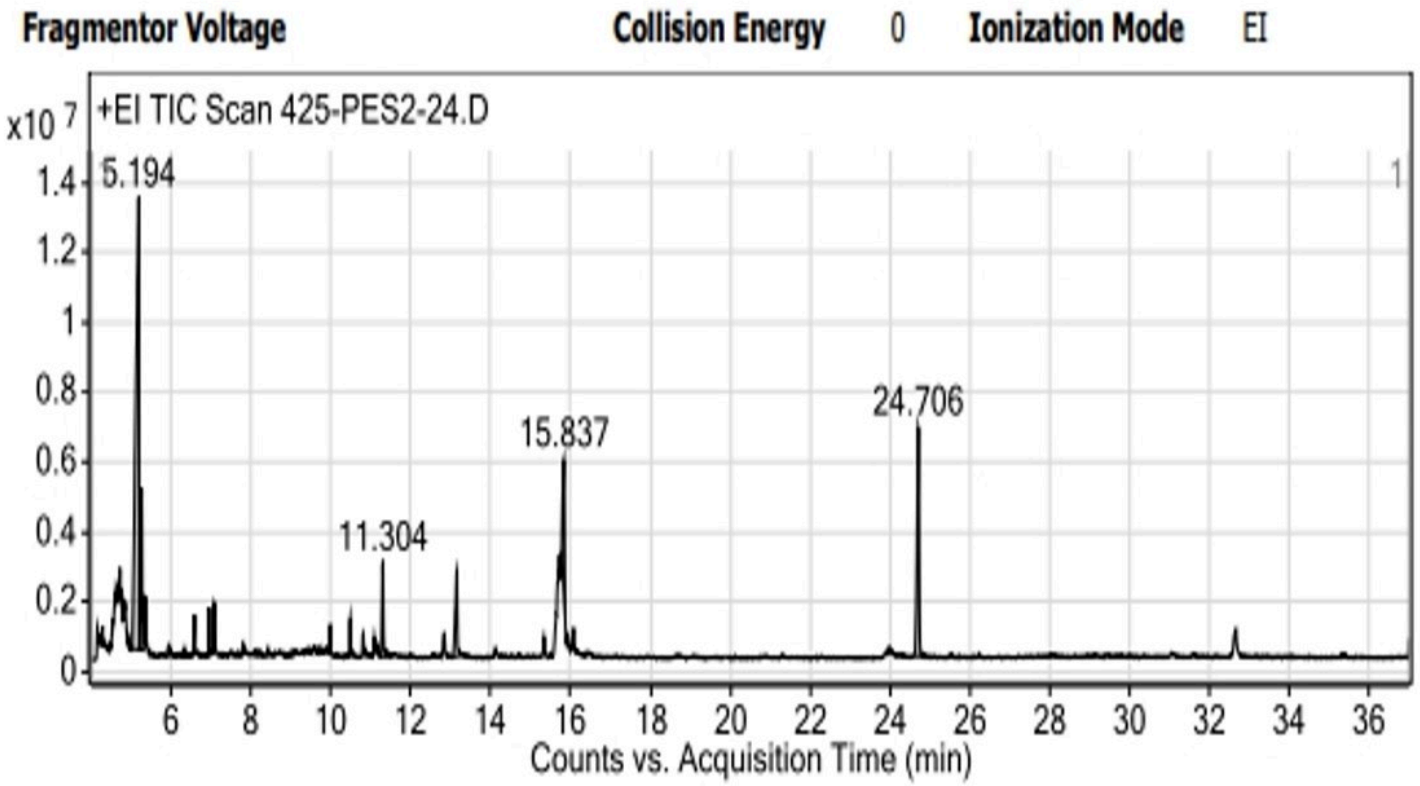


Figure 6

A chromatogram of the retention times of the compounds present in the acetonitrile extract of kale.

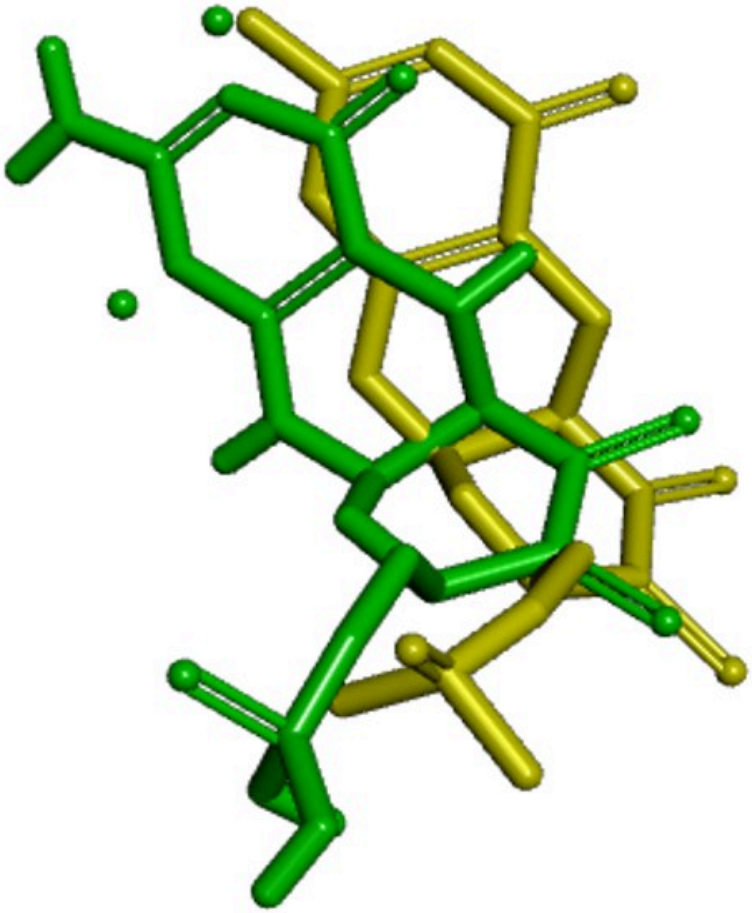


Figure 7

Superimposition of the Ligands of the co-crystallized structure (yellow) and the redocked structure (green) to determine the RMSD.

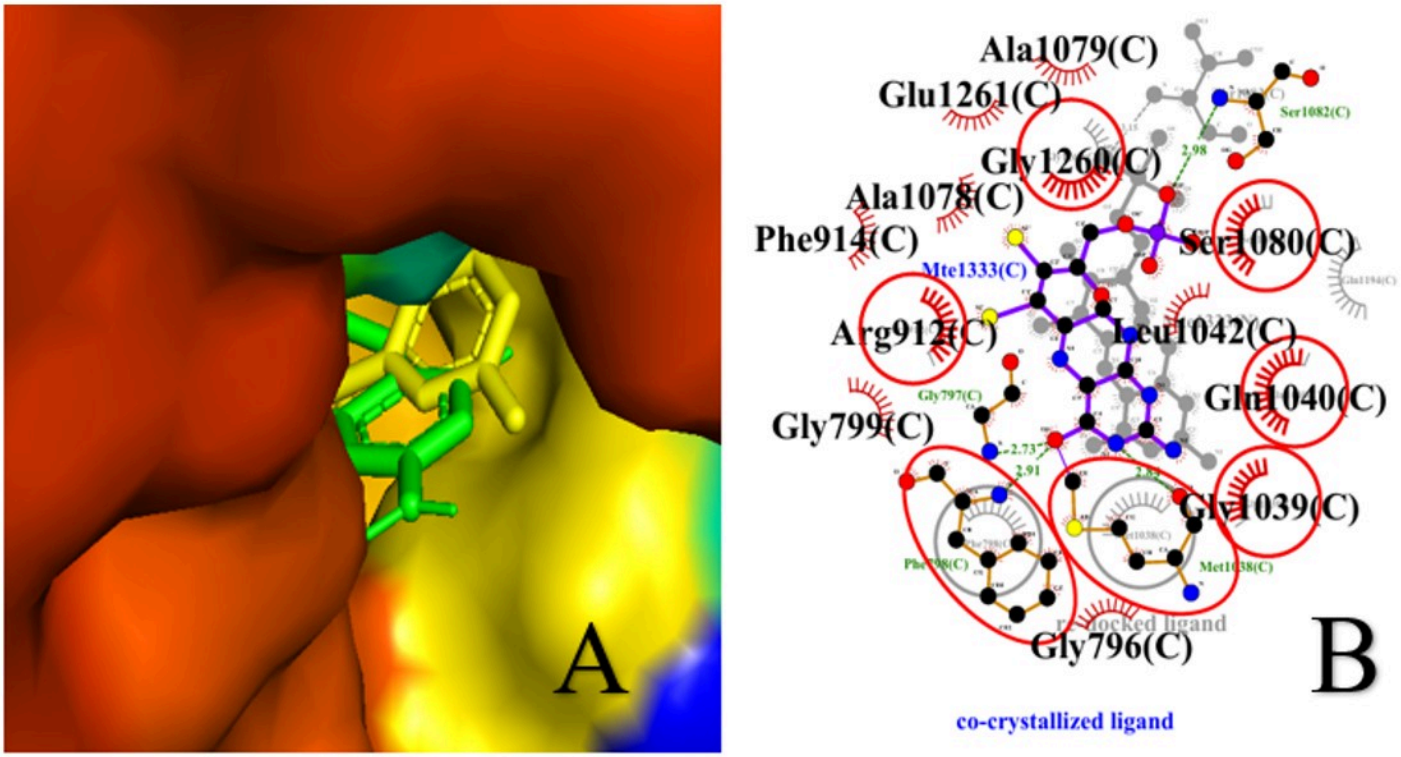


Figure 8

PyMol representation of 1FIQ depicting the co-crystallized ligand (yellow) and the re-docked ligand (green) within the binding pocket (A) and 2D superimposed LigPlot+ diagram (B) showing the overlapping interactions between the co-crystallized and re-docked ligands. Residues involved in both binding modes are highlighted with red circles.

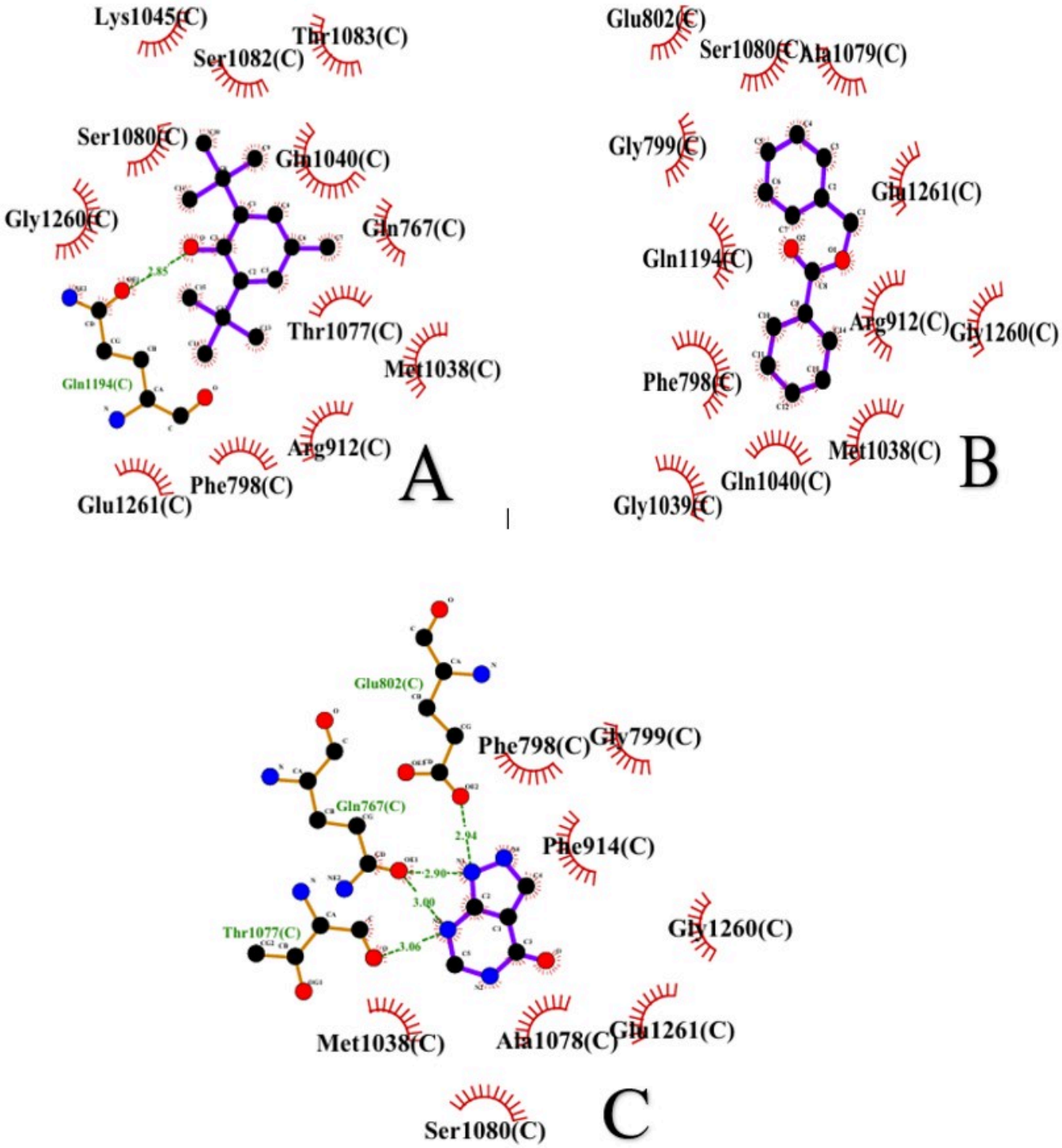


Figure 9

Protein-ligand interaction of (A) 1FIQ- PubChem ID 31404, (B) 1FIQ- PubChem ID 2345, and (C) 1FIQ- reference drug complexes.

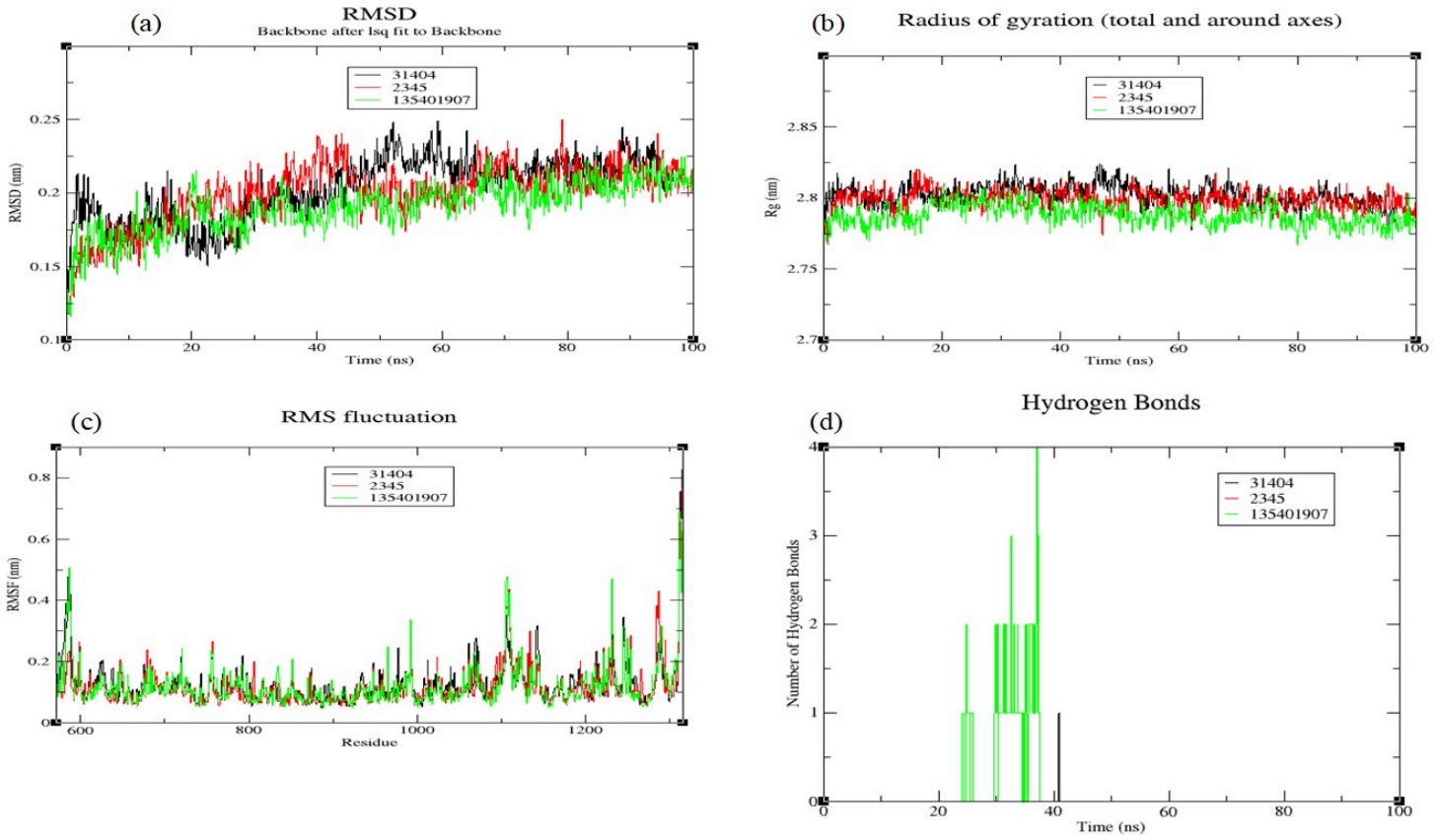


Figure 10

Results from the molecular dynamics simulations studies compute (a) RMSD, (b) Rg, (c) RMSF and (d) HB for the protein-ligand complexes

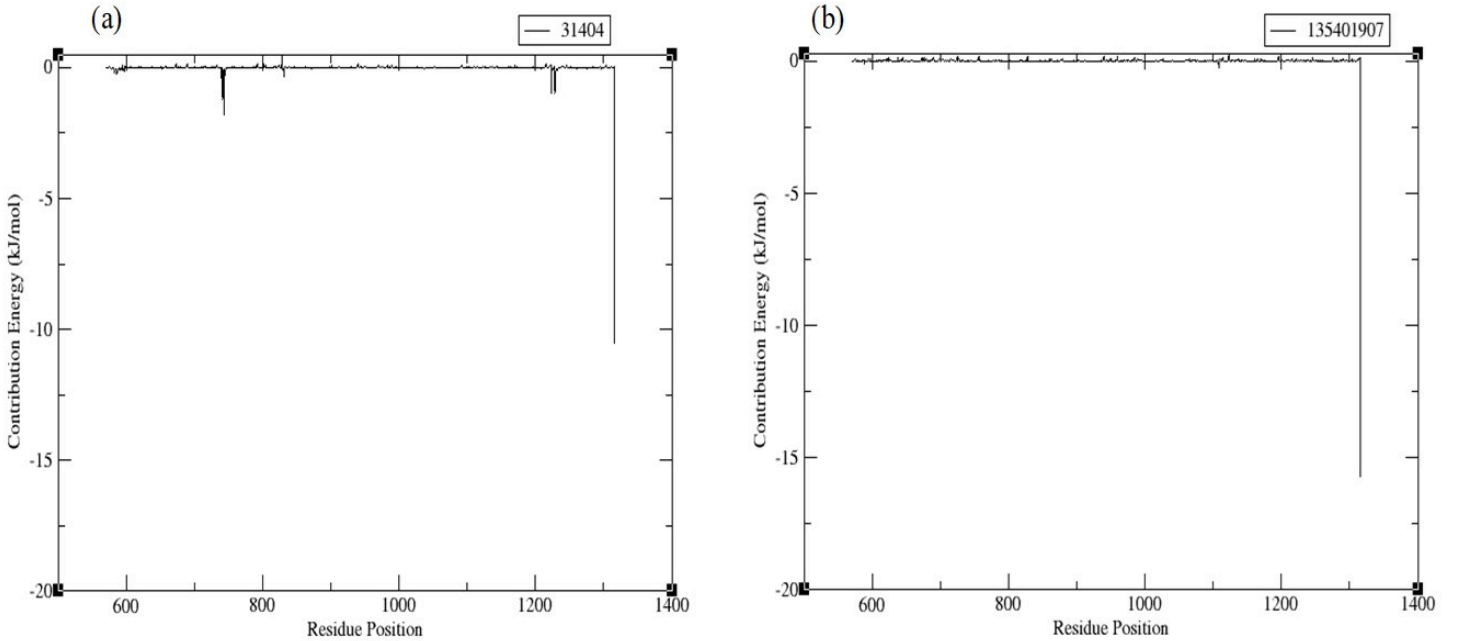


Figure 11

Results from the per-residue decomposition studies for the complexes of (a) 31404 and (b) 135401907